UNIVERSITY OF OKLAHOMA

GRADUATE COLLEGE

INTERRELATING PRODUCTION ANALYSIS WITH PORE SCALE STRUCTURE IN THE BAKKEN RESERVOIR

A THESIS

SUBMITTED TO THE GRADUATE FACULTY

in partial fulfillment of the requirements for the

Degree of

MASTER OF SCIENCE

By

MIGUEL ANGEL GRELLA
Norman, Oklahoma
2016

INTERRELATING PRODUCTION ANALYSIS WITH PORE SCALE STRUCTURE IN THE BAKKEN RESERVOIR

A THESIS APPROVED FOR THE
MEWBOURNE SCHOOL OF PETROLEUM AND GEOLOGICAL ENGINEERING

BY

_____
Dr. Jeffrey Callard, Chair

_____
Dr. Mashhad Fahs

_____
Dr. Ahmad Sahaee-Pour

To my wife Carolina who had the patience and dedication to take care of our children while completing all my graduate studies.

Acknowledgements

First and foremost I must thank God to provide me with health, skills and drive to finish this highly sought goal.

I also want to express my gratitude to my employer Continental Resources who gave me the opportunity to advance my skill set thru several years of service and gave me invaluable petroleum engineering experience in the Bakken formation.

Special thanks to Dr. Jeff Callard for his guidance and unconditional availability thru the process of completing this work.

I would also like to thank Dr. Fahs and Dr. Sakhaee-Pour for being a part of my thesis committee and providing generous feedback for the final stage of this work.

Thanks to Dr. Deepak Devegowda and the staff of the Mewbourne School of Petroleum and Geological Engineering who diligently provided their time and guidance for the advancement of administrative processes.

Table of Contents

List of Tables

List of Figures

Abstract

Improving well performance and associated project economics in oil resource plays rely on developing reservoir characterization capabilities. The need for understanding pore-scale geometry in low porosity low permeability reservoirs has only recently become of importance owing to the now commerciality of these reservoirs through the enabling technology of multi-stage fracture stimulation in horizontal wells.

Conventional laboratory analysis of multi-phase flow in low porosity low permeability systems becomes unpractical with reduced permeability. However, from conventional reservoir characterization, deriving relative permeability from pore structure models utilizing capillary pressure measurements is possible with modern high pressure mercury capillary pressure equipment. Applicability of this method was successfully evaluated by history matching, using numerical simulation, dependent on capillary pressure derived relative permeability and compared to field production in the Bakken formation in North Dakota.

Other useful results from the combination numerical simulation and field production data study include the prediction and observation of an elevated yet constant producing gas oil ratio during the linear flow period (prior to boundary dominated flow.) This observation prevents incorrect recombination ratios for fluid characterization when flowing pressure is below saturation pressure and also prevents faulty calculations of formation volume factor and saturation pressure. Furthermore, the

elevated constant production gas oil ratio may be used itself to predict relative permeability.

1 Introduction

1.1. Background

Relative permeability is an essential input parameter in many areas of reservoir engineering and is particularly fundamental to calibrate numerical reservoir simulation models through production history matching techniques in order to strengthen reserve forecasting capabilities and improve well performance. However, due to the complexity of interactions among the fluid phases and the rock fabric itself, there is not a universal formulation able to predict 2 phase relative permeability for a wide range of wettability and rock properties.

The techniques to calculate relative permeability from capillary pressure were developed in late 1940. However, the application to tight rocks was not fully employed until the equipment was able to reach the elevated pressures necessary to drain the tiny Nanopores.

1.1.1 Methods of Relative Permeability Measurements

Relative Permeability versus saturation relationships are obtained by conducting multiphase flow experiments in the laboratory. The measurements are typically conducted on a plug of defined dimensions that has to be carefully machined from a larger core.

Delicate economics in unconventional resource plays prevents that costly process of core extraction and routine core analysis, therefore when available cores are scarce and uncommon.

Core Microcracking has been reported to be a common issue with the core retrieval processes in tight rocks, the complexity of the rock fabric and the weak interfaces between organic/inorganic facies are often cracked or sheared due to stress unloading and hydrocarbons expansion. This microcracking results in fissures of high conductivity that provide unrealistic high permeabilities and inconsistent results. (Handwenger et al., 2012)

Several researchers have proposed different methods for the determination of relative permeability in the laboratory, but in general the experiments can be classified in either “Steady State” or “Unsteady State” displacement tests. Due to the inherent setup required for testing, a capillary discontinuity or artificial boundary is created when fluids pass from the outlet end of the sample core plug to the end piece of the testing apparatus. This discontinuity creates a bank of wetting fluid at the end piece of the sample which affects the saturation distribution and pressure drop required to obtain meaningful relationships. This phenomenon is commonly termed capillary end-effect (CEE) and has been studied extensively; some authors have proposed techniques to correct for this error in steady states tests (Gupta, R., & Maloney, D. R., 2014)

Steady State measurements are typically forbidden in low porosity low permeability applications as the methodology requires an accurate determination of in situ saturation after each displacement level reaches equilibrium, which can take in the order of weeks to months to reach for a single saturation point.

Unsteady test measurements do not require equilibrium to be reached, but require accurate monitoring of injection rates and pressure drop across the core, as they rely on pressure decay as an input in the mathematical formulation used to derive fractional flow. The main disadvantages of this method are rate dependent instability effects and potential non-equilibrium between displacing and displaced fluids. (Thomas et al., 1991)

1.1.2 Factors Affecting Relative Permeability Measurements

Relative permeability functions are affected by many factors including but not limited to fluid phase saturations, wettability, interfacial tensions, rock fabric, saturation history, clays and fines content and temperature (Behrenbruch, P., & Goda., 2006).

Wettability and phase behavior of low porosity low permeability reservoirs is difficult to describe and not well understood mainly due to the spatial confinement in which reservoir fluids are subjected within the highly complex pore structure. The literature reports changes in phase behavior and fluid properties when fluids are subjected to such tiny spaces in which the intermolecular forces cannot simply be ignored (Sapmanee, 2011). In addition the presence of both organic and inorganic

material within the rock fabric could be conducive to conditions in which wettability could be preferential to either the oleic or the aqueous phase depending on whether the pore space contains silicate minerals, calcite, clays, organic matter, or a combination of all of these (Figure 1).

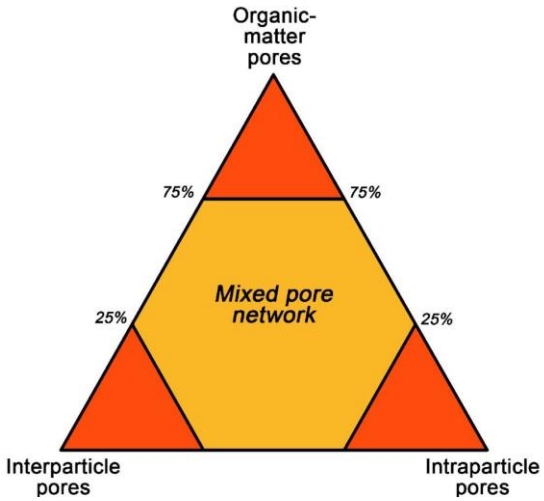

Figure 1. Three end-member classification of pore types. Loucks et al., 2010

A detailed discussion about how Nano and Mesopore scales affect phase behavior and the outcome of relative permeability values is beyond the scope of this work. However geological heterogeneities vary across micro and macro scale, and the finding a common ground between production behavior and advanced core analysis can certainly augment our predictive capabilities for well performance and reserve forecasting.

1.1.3 Objectives

The purpose of this work is to extend the application of relative permeability derived from pore throat models and correlate between model predicted and field observed point values of hydrocarbon production during the linear flow period. The procedure which utilizes laboratory mercury injection capillary pressure from core samples from the Bakken reservoir is used to generate a distribution of wetting phase saturation exponents and residual wetting phase saturations for simulation model input and correlate the saturation exponents with the Cumulative Oil production and time to reach linear flow.

Additionally, a comparison of the relative permeability distributions derived from laboratory and the relative permeability distributions of well performance are examined to determine the extent of the relationship.

1.2 Geological Setting of Williston Basin

1.2.1 Introduction to the Middle Bakken

The Williston basin was a partial unified intracratonic basin located in the northwest of North America, the US portion of the basin primarily underlays significant areas of the state of North Dakota and Montana. The depression of roughly elliptical shape measures approximately 475 miles north-south and 300 miles east-west, and has a maximum depth of nearly 16,000 feet in the center, beneath McKenzie County, ND.

It is generally accepted that oils produced from both the Bakken and the Three Forks Formations were originally generated in the Bakken Formation (Petty, 2014; Gaswirth et al., 2013; Bottjer et al., 2011).The Bakken Formation consists of three members, a middle mixed carbonate-siliciclastic member, confined between upper and lower organic-rich black shales members. It can be further subdivided into 11 facies that were deposited during the late Devonian period to early Mississippian, ten of which characterize the middle Bakken member and the other forms the lower and upper Bakken black shale members.

Figure 2 depicts white light photographs of cored facies:

A - Organic-rich black shale (facies 1)

B - Inorganic siliciclastic silt- to mudstone (facies 2)

C - Nereites siltstone (facies 3)

D - Intercalated sandstone/siltstones with siliciclastic mudstone (facies 4)

E - Macaronichnus siltstone (facies 5)

F - Horizontally-laminated siltstone (facies 6)

G - Massive, horizontal and cross-bedded sandstone (facies 7)

H - Quartz sandstone with ooids (facies 8)

I - Laminated cyanobacterial bindstone (facies 9)

Figure 2. Facies of the Bakken Formation

According to data collected by the U.S. Energy Information Administration (EIA) Bakken and Three Forks formations in the Williston Basin are ranked as the second most prolific tight oil reservoirs in the United States after the Eagle Ford (Figure 2). The North Dakota Industrial commission (NDIC) reports that the Middle Bakken formation accounts for more than 45% of the state of North Dakota cumulative oil production and has already surpassed 1,590,000,000 barrels of oil thru December 2015. (Table 1)

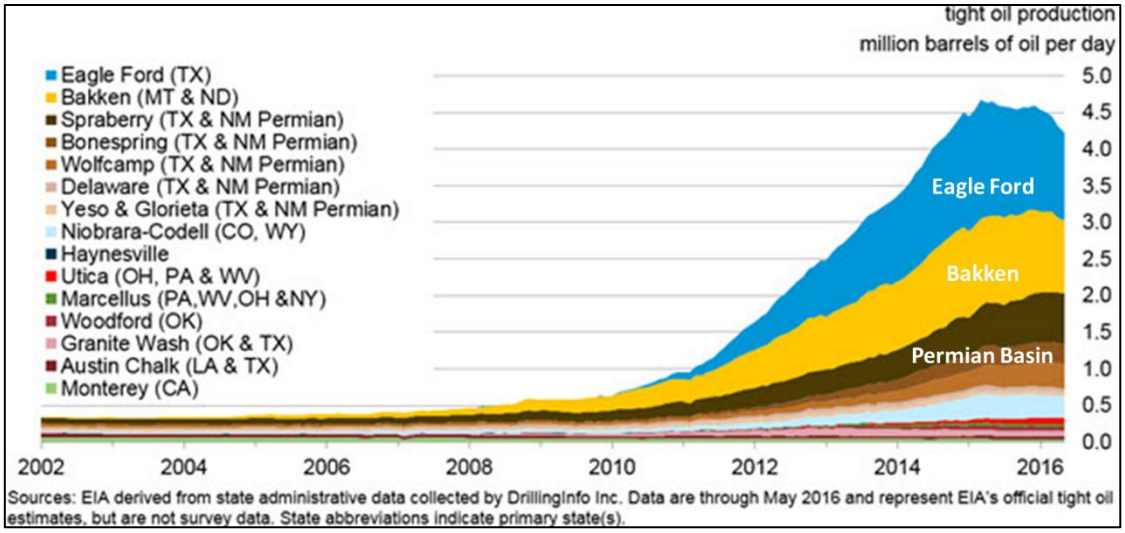

Figure 3. U.S. Tight Oil Production from Selected Plays

Table 1. North Dakota Cumulative Oil Production by Formation through December 2015 (NDIC website)

FORMATION	CUMULATIVE OIL [stb]	PERCENT	WELLS
BAKKEN	1,590,525,938	46.9581	10,930
BAKKEN/THREE FORKS	10,268,622	0.3032	53
BIRDBEAR	20,708,932	0.6114	174
CAMBRO/ORDOVICIAN	436,287	0.0129	5

2 Laboratory Core Analysis

For shale oil resource systems as the Petroleum Bakken System, the generated oil is either stored in the organic-rich mudstone intervals or migrated into juxtaposed, continuous organic-lean intervals, Middle Bakken. Due to the nature of the depositional processes multiple lithofacies are stacked resulting in a broad classification of facies with potentially different rock properties.

Permeability methods previously defined measure bulk permeability which is susceptible to the heterogeneity of the system and the presence of microcracks. Most models for prediction of permeability using mercury injection capillary pressure (MICP) rely only on porosity and pore size distribution and therefore are inherent to the core sample integrity (Li et al., 2015).

Modern MICP equipment is capable of reaching mercury injection pressures of up to 60,000 psi. This is roughly equivalent to pore throat sizes of around 2 ηm in radius which covers the full range of pore sizes encountered in the Bakken reservoir (Figure 4)

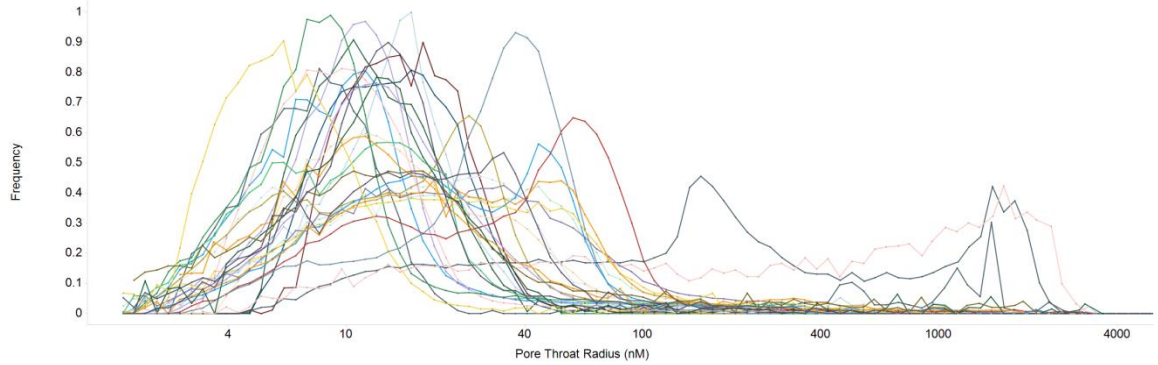

Figure 4. Pore size distribution of Middle Bakken samples used for the study

2.1 Sample Selection and Core locations

Mercury injection capillary pressure tests were conducted on 38 plug samples extracted from 10 vertical cores retrieved throughout the basin (Figure 5). All samples were extracted from the Middle Bakken member and tested by a commercial laboratory. Helium porosity was also recorded on the same sample set. Fractured samples are not accounted and were excluded from our findings. Table 2 shows average true vertical depth (TVD) of samples and county in which the well was drilled. Well names have been omitted due to confidentially reasons.

Table 2. Average TVD and county location of vertical cores used in the study

Core	County	Average Sample Depth [ft]
1	Stark , ND	10,766
2	Williams, ND	10,624
3	Williams, ND	10,755
4	Burke, ND	9,215
5	Dunn, ND	11,106
6	Williams, ND	9,186
7	McKenzie, ND	11,305
8	Richland, MT	10,105
9	Richland, MT	11,063
10	Divide, ND	9,283

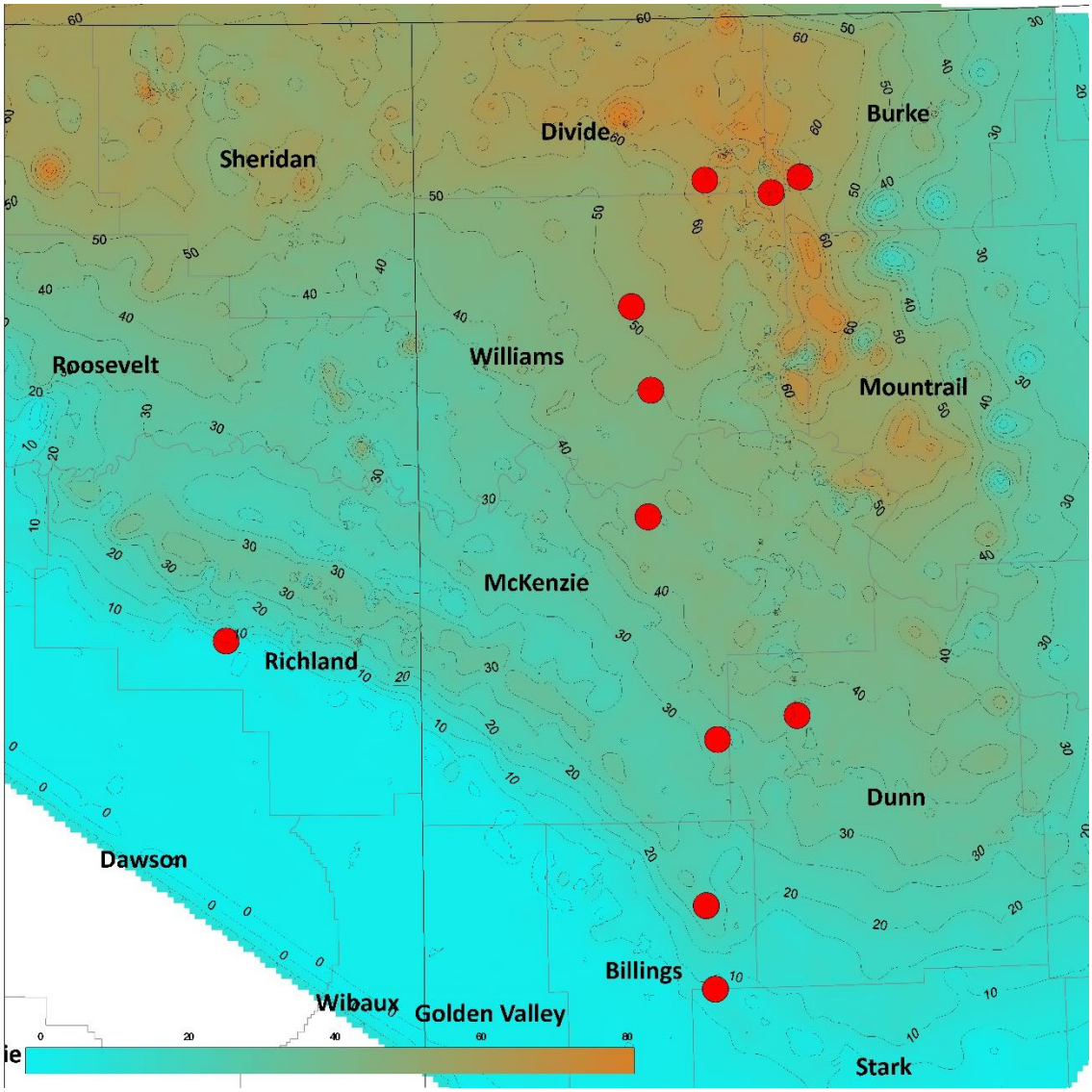

Figure 5. Middle Bakken Isopach of the Williston Basin indicating the location of cores used for the study.

2.2 Pore Structure Characterization using Mercury Injection Capillary Pressure

In 1960 Thomeer observed that capillary pressure curves acquired from rocks with similar characteristics form a family. He also noted differences between the shapes and location of the capillary pressure curves that provided some indication of pore geometry and a degree of interconnection of the pore structure. The proposed method indicated that when mercury injection capillary pressure (P_c) was plotted vs. the

fractional bulk volume occupied by mercury (S_b) on a log-log scale the resulting curve will approximate that of a square hyperbola with the following equation:

$$\frac{S_b}{S_{b\infty}} = e^{-\frac{F_g}{(\frac{logP_c}{P_d})}} \quad (1)$$

The location of the hyperbola will be determined by its asymptotes which would have values defined by the percent bulk volume occupied by mercury at infinite capillary pressure, $S_{b\infty}$ and mercury/air extrapolated displacement pressure, P_d. The shape of the curve was defined by a parameter F_g termed "pore geometrical factor." According to Thomeer, this factor would provide a degree of the distribution of pore throats and the associated interconnected pore volume. Furthermore, each capillary pressure curve could be uniquely identified by all three parameters as shown in Figure 6

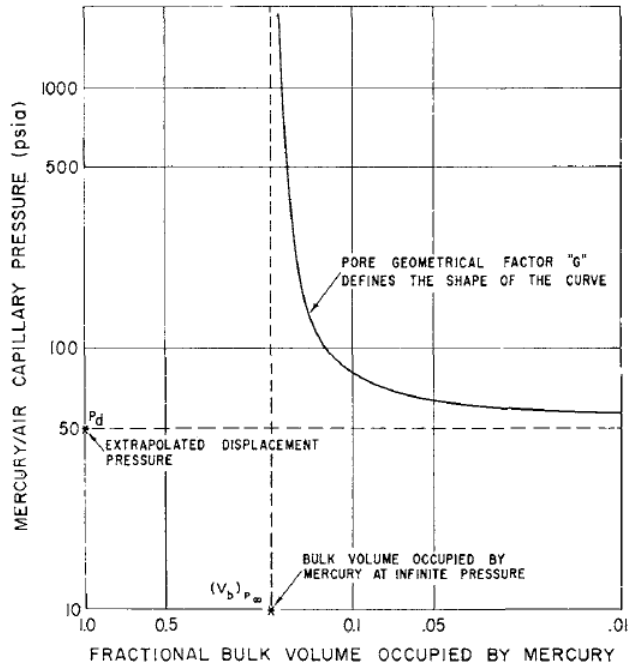

Figure 6. Definition of pore-network parameters described by Thomeer (1960) to approximate MICP curve to a hyperbola

2.3 Exclusion of Non-Intrusive Data and Hyperbolic Match

Capillary pressure curves for Middle Bakken samples were studied and a numerical determination of all three pore-network parameter was conducted according to a graphical method. A synthetic hyperbola was generated using initial values for the parameters of equation 1. Final values were found by matching the synthetic hyperbola to the lab data. Examples for samples 2-13 and 2-1-1 are given in Figures 7 and 8.

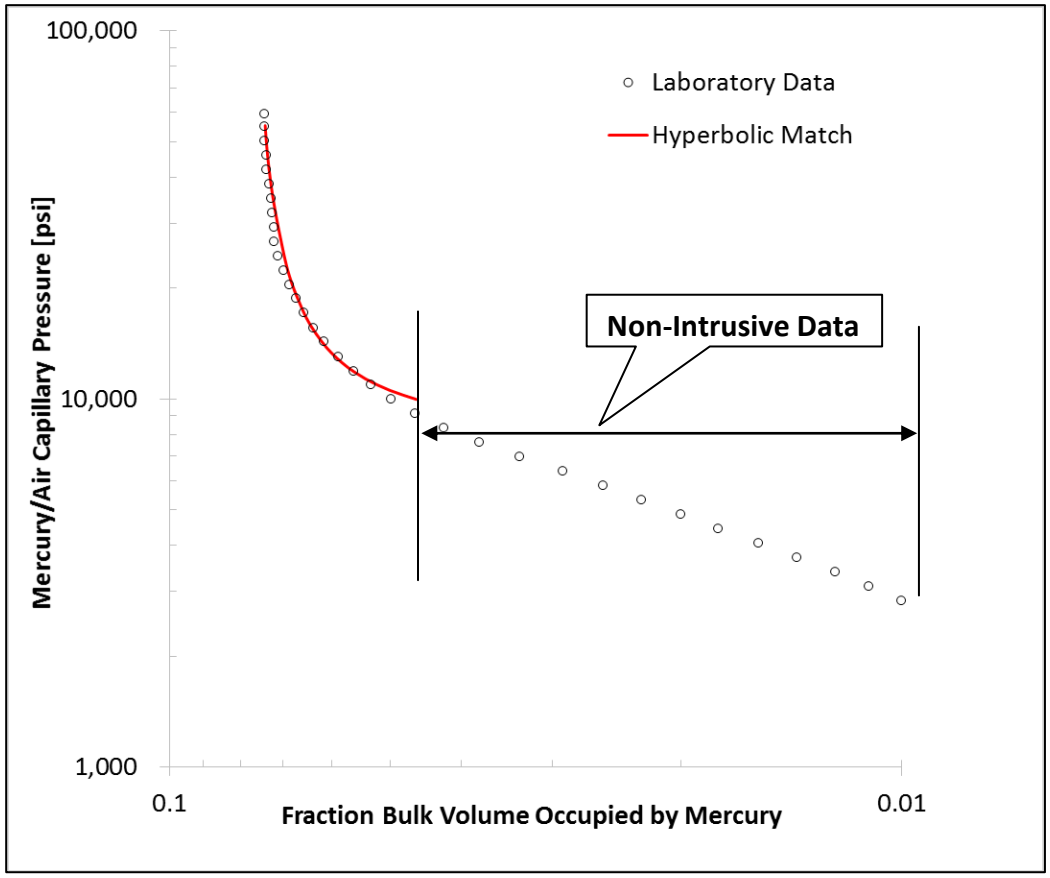

Figure 7. Detail of hyperbolic match of MICP data sample 2-13

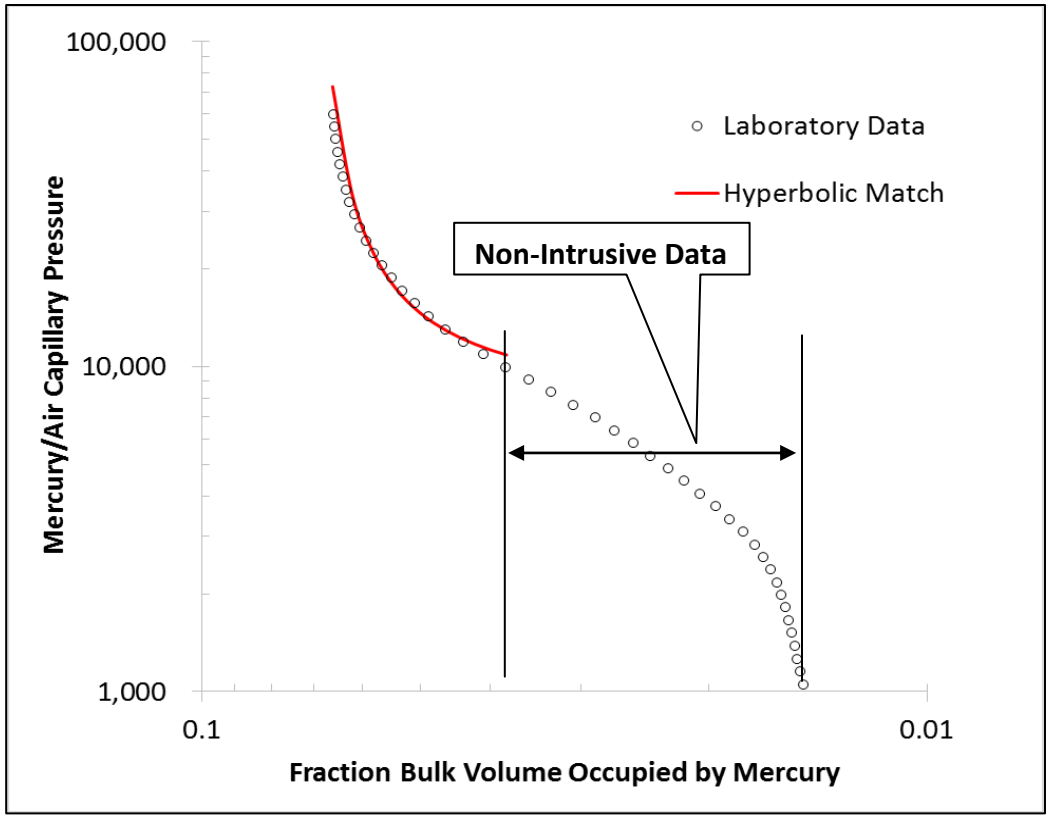

Figure 8. Detail of hyperbolic match of MICP data sample 2-1-1

Note that the capillary pressure curves exhibit both a low and a high-pressure hyperbola. For tight rocks the low-pressure hyperbola describes effects of closure as mercury conforms to the roughness of the sample. Closure or conformance is caused by plucked grains, coring induced fractures and saw marks. (Bailey, 2009). The high-pressure portion of the curve selected for the match represents the volume of mercury that has finally been able to drain the interconnected pore structure once that capillary pressure reaches a value high enough to intrude the largest pore.

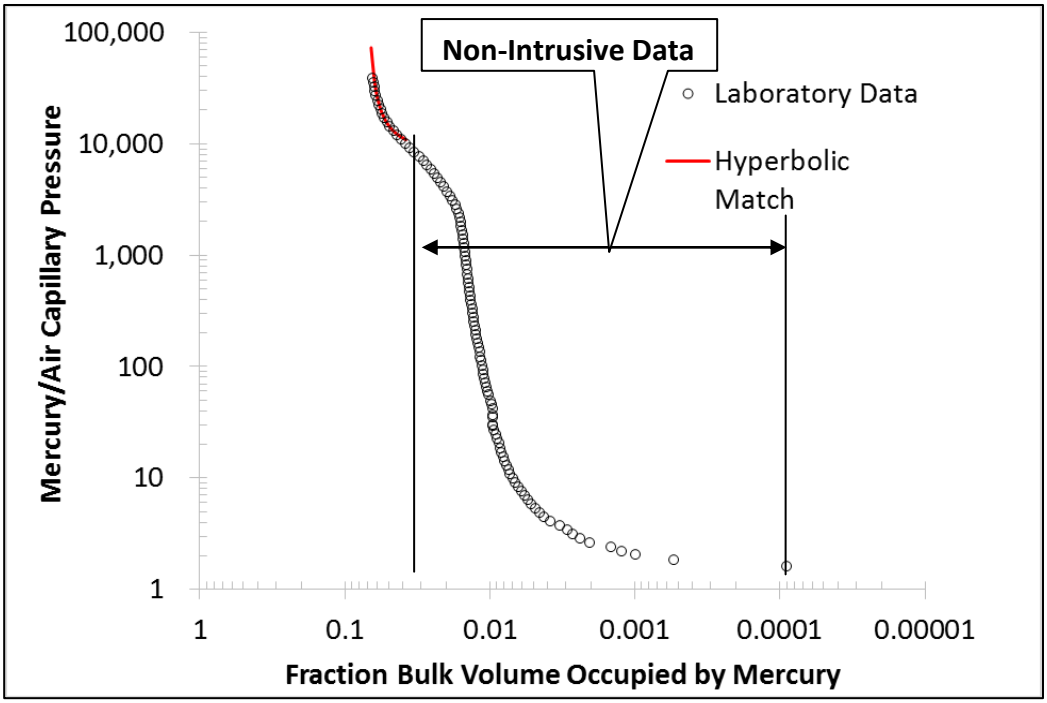

Figure 9. Hyperbolic match of MICP data sample 2-1-1

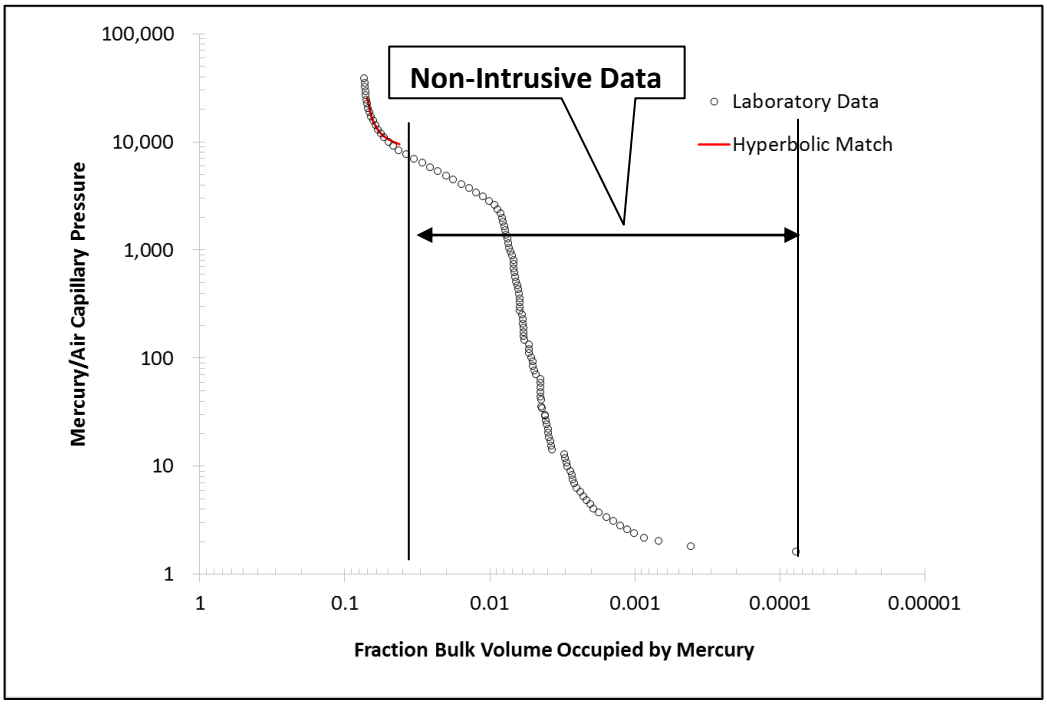

Figure 10. Hyperbolic match of MICP data sample 2-13

Figure 11 overlays the capillary pressure data of our study samples over the family of capillary pressure curves computed by Thomeer (1960). Table 3 summarizes pore-network parameters determined for all samples used in the study.

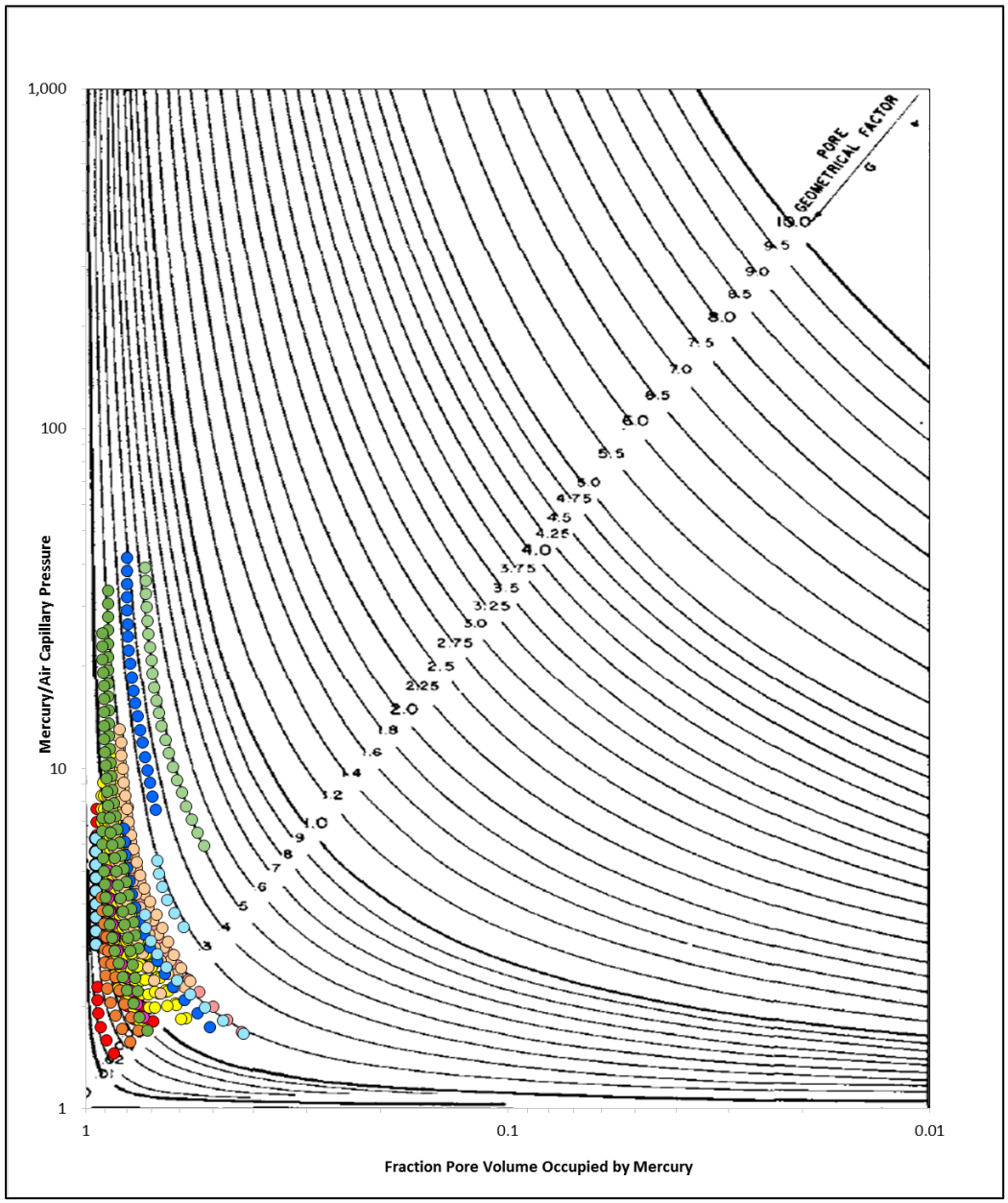

Figure 11. Laboratory data for study samples over family of capillary pressure curves computed by Thomeer (1960).

Table 3. Pore-network parameters determined for Middle Bakken Samples used in the study

Sample No.	F_g	$S_{b\infty}$	P_d
1-67	0.19	1.3%	6,500
1-115	0.13	3.5%	6,500
1-74	0.06	1.7%	8,500
1-79-1	0.06	7.7%	5,500
2-5	0.02	3.0%	22,000
2-7	0.08	7.8%	7,200
2-13	0.08	8.1%	7,200
1-86	0.13	7.5%	7,000
2-1-1	0.13	7.5%	7,000
2-1	0.12	7.0%	5,000
2-9-1	0.14	8.9%	4,500
2-9	0.06	4.4%	13,000
2-20	0.07	7.1%	6,000
2-26	0.11	4.2%	7,000
2-40	0.09	7.8%	5,500
2-49-1	0.10	6.8%	6,000
2-55	0.11	3.8%	8,500
2-55-1	0.13	5.4%	5,500
2-60	0.13	5.5%	6,000
1-75	0.07	7.2%	10,000
1-83	0.08	5.2%	10,000
1-93	0.08	6.1%	11,000
1-64	0.11	8.4%	6,000
1-68	0.13	7.9%	5,000
2-5	0.19	10.0%	4,000
2-9	0.16	10.2%	4,000
2-19	0.20	12.0%	4,200
1-88	0.31	6.3%	1,200
1-100	0.15	6.4%	7,500
1-55	0.16	4.2%	6,000
1-56	0.27	2.8%	3,800
1-58	0.02	4.0%	8,000
1-71	0.04	2.2%	13,000
1-77	0.06	3.5%	12,000
1-54	0.07	7.8%	7,000
1-67	0.15	4.9%	1,500
1-71	0.12	10.5%	2,000

2.4 Conversion to Relative Permeability

Wang et al., 2012 performed a wettability study on the Middle Bakken cores and determined the initial wettability state of the cores in his study was generally oil - wet. In an oil-wet system, the continuous phase can be assumed to be the oleic phase, as gas evolves it will preferentially move to the center of the pore as conceptually represented in the Alharthy et al., 2013 for a bubble-point fluid system (Figure 12)

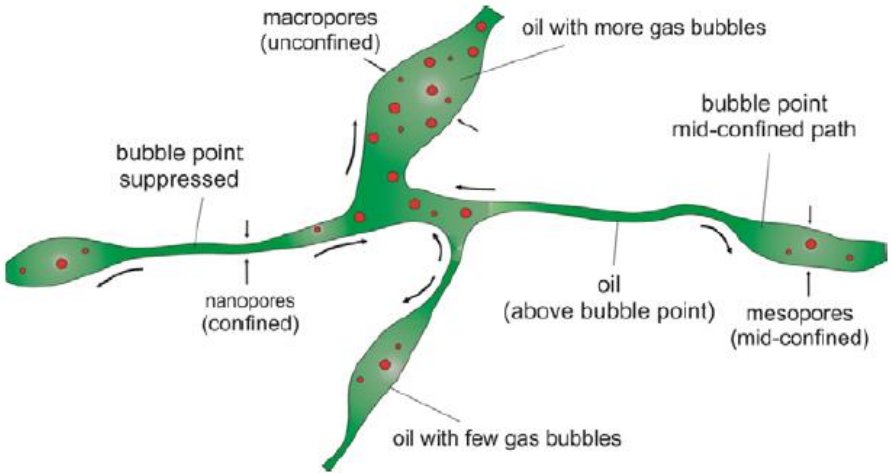

Figure 12. Conceptual pore network for a bubble-point oil-wet system in which the fluids exhibits different phase behavior in different pore sizes. Alharthy et al., 2013

In 1949 Purcell proposed the following equation to estimate air permeability using mercury injection:

$$K_a = 10.6566[\sigma cos\theta]^2 F_1 \phi \int_0^1 \frac{dS}{{P_c}^2} \qquad (2)$$

The theory behind its derivation approximated flow in porous media to a bundle of capillary tubes and related the capillary pressure to the radius of the tubes using both

the air-mercury interfacial tension σ and the contact angle of the mercury phase. The parameter F_1 was introduced to account for the effect of rock tortuosity and the deviation between observed and the bundle of capillary tubes model.

In 1951, Fatt and Dykstra, based on Purcell's work, assumed a value for the constant $b = {}^{1}/_{2}$ which expressed the tortuosity as a function of the pore radius and therefore dependent of saturation. The relative permeability could be expressed as follows:

$$K_r = \frac{\int_0^S \frac{dS}{{P_c}^3}}{\int_0^{100} \frac{dS}{{P_c}^3}} \tag{3}$$

Equation 3 can be expressed in terms of an equivalent oil-gas system in which oil is the wetting phase S_w and mercury saturation is the non-wetting phase (Table 4). Upon integration of the capillary pressure in terms of the three pore-network parameters, the resulting relative permeability can be plotted vs. the wetting phase saturation as shown in Figure 13.

Table 4. Equivalent Systems assumed for the conversion of relative permeability

System	Wetting Phase S_w	Non-wetting Phase S_{nw}
Air- Mercury	Air	Mercury
Oil- Gas	Oil	Gas

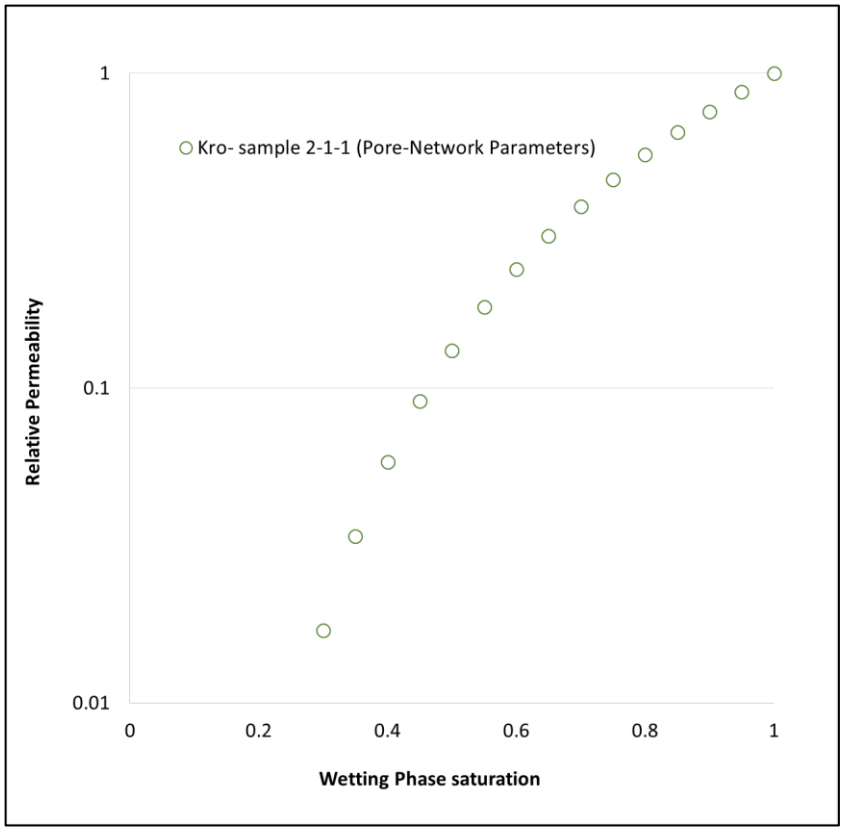

Figure 13. Oil relative permeability curve generated from pore-network parameter of sample 2-1-1. $F_g = 0.13, S_{b\infty} = 7.5\%, P_d = 7000\ psi$

2.5 Fit to Model Wetting Phase Saturation Exponent and Irreducible Wetting Saturation

The Brooks-Corey formulation is perhaps the most widely used relationship empirically describing how the relative permeability changes in the presence of partially saturated porous media, it is used extensively in the industry and its wide acceptance more likely relies on the practicality in which the laboratory derived relationships are expressed in terms of simple power functions .

Corey's initial model was based on experimental data and proposed the calculation of relative permeability for an oil-gas system using the following set of equations:

$$K_{ro} = (S_{oe})^4 \quad (4)$$

$$K_{rg} = (1 - S_{oe})^2(1 - {S_{oe}}^2) \quad (5)$$

$$\text{where } S_{oe} = \frac{S_o - S_{or}}{1 - S_{or}} \quad (6)$$

After almost ten years Corey and Brooks [5, 6] realized that a log-log plot of normalized oil saturation S_{oe} vs. capillary pressure P_c yielded a straight line of slope λ.

$$S_{oe} = (P_d/P_c)^{\lambda} \quad (7)$$

This finding allowed Corey to rewrite his original formulation to express relative permeability of the non-wetting phase K_{rnw} if both the wetting phase saturation and the term λ were known.

$$K_{rw} = (S_{oe})^{\frac{2+3\lambda}{\lambda}} \quad (8)$$

$$K_{rnw} = (1 - S_{oe})^2(1 - S_{oe}^{\frac{2+\lambda}{\lambda}}) \quad (9)$$

As proposed by Lake (1989) equations 8 and 9 can be further simplified if we allow exponents to define the curvature of the relative permeability functions. In this case the Corey exponent for the wetting phase is defined by:

$$n_w = \frac{2+3\lambda}{\lambda} \tag{10}$$

and the Corey exponent for non-wetting phase can be defined in a similar fashion as:

$$n_{nw} = \frac{2+\lambda}{\lambda} \tag{11}$$

Algebraic manipulation of equations 10 and 11 allow us to establish the following relationship between n_w and n_{nw} for all values of λ:

$$n_{nw} = n_w - 2 \tag{12}$$

Finally, for an oil-gas system, equations 8 and 9 can be expressed in terms of the wetting phase saturation exponent only:

$$K_{ro} = (S_{oe})^{n_o} \tag{13}$$

$$K_{rg} = (1 - S_{oe})^2 (1 - S_{oe}{}^{(n_o - 2)}) \tag{14}$$

In our study, we investigated how the Corey-Brooks model approximated to the relative permeability function described by the pore-network parameters. The procedure involved plotting both curves over the same wetting phase saturation range and using numerical regression to find values of S_{or} and n_o that simultaneously provided the best fit to the data. Figure 14 exemplifies the curve match achieved for sample 2-1-1.

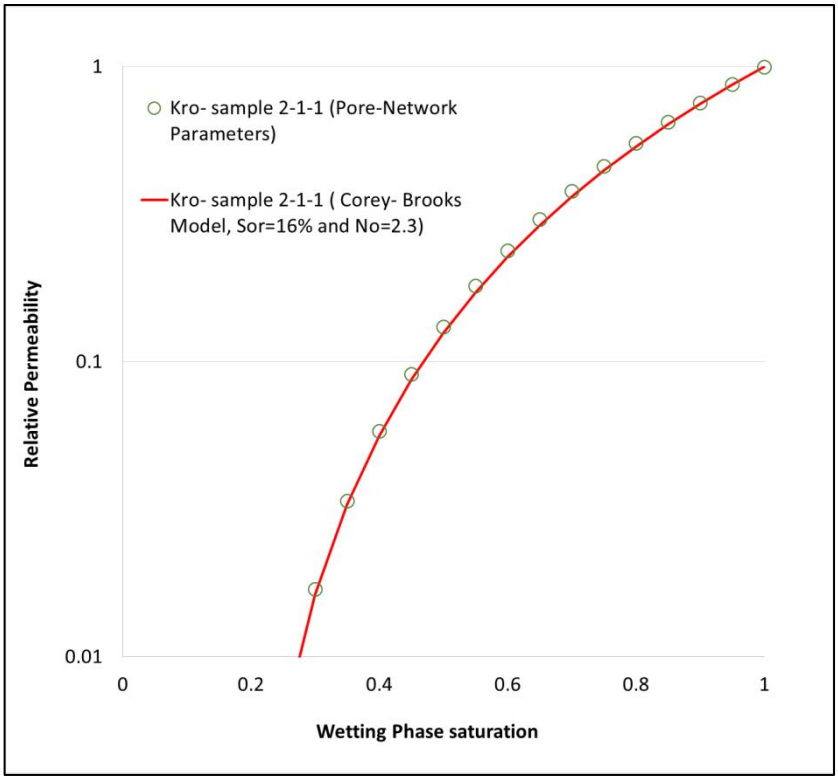

Figure 14. Match between Corey-Brooks Model and Pore-Network Parameter Relative Permeability function for sample 2-1-1. $S_{or} = 16\%,\ n_o = 2.3$

It is noteworthy to indicate that using both S_{or} and n_o to achieve a fit, resulted in a more robust match to the experimental data. Neglecting a value of residual oil saturation resulted in a different value of $n_o$to be found and only allowed a partial match thru the high oil saturation range. Figure 15.

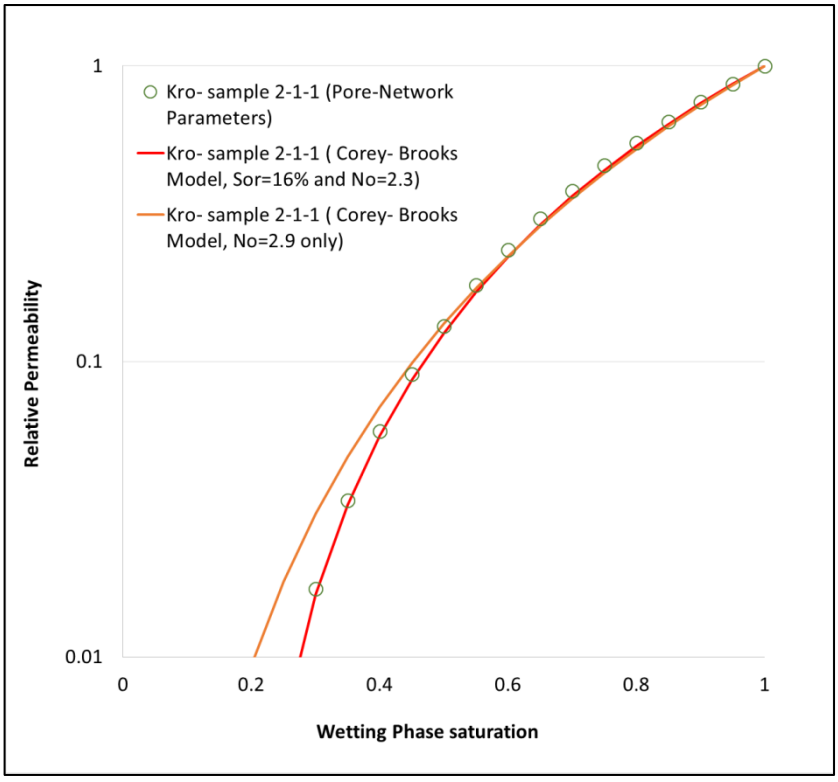

Figure 15. Comparison of Corey-Brooks function match to experimentally derived relative permeability. Note fit throughout full wetting phase range is not possible when residual oil saturation is neglected (orange line)

All core samples were analyzed using the methodology discussed above. Table 5 summarizes all values of S_{or} and n_o. Further insight in the values of wetting phase saturation exponent reveal a distribution of n_o exponents ranging approximately between values of 1 to 4. Figure 16.

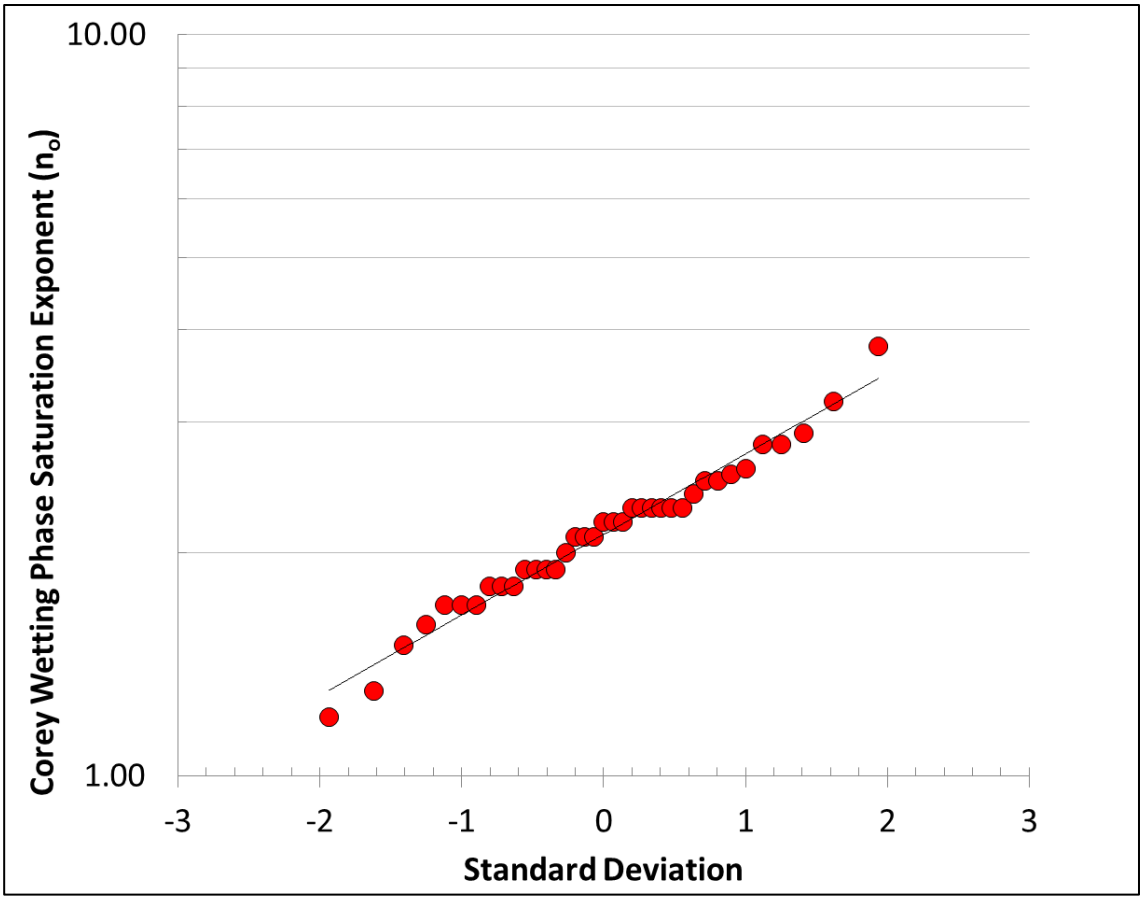

Figure 16. Normalized distribution of wetting phase exponent derived from laboratory core analysis

Table 5. Corey oil saturation exponent and residual oil saturation determined through a fit of experimental data.

Sample No.	n_o	S_{or}
1-67	2.90	15.0%
1-115	2.30	15.0%
1-74	1.60	14.0%
1-79-1	1.70	11.0%
2-5	1.20	10.0%
2-7	1.90	10.0%
2-13	1.80	14.0%
1-86	2.30	16.0%
2-1-1	2.30	16.0%
2-1	2.20	15.0%
2-9-1	2.50	14.0%
2-9	1.70	12.0%
2-20	1.80	12.0%
2-26	2.20	13.0%
2-40	2.00	13.0%
2-49-1	2.10	14.0%
2-55	2.10	15.0%
2-55-1	2.30	15.0%
2-60	2.30	15.0%
1-75	1.80	12.0%
1-83	1.90	12.0%
1-93	1.90	11.0%
1-64	2.10	15.0%
1-68	2.30	15.0%
2-5	2.80	16.0%
2-9	2.55	16.0%
2-19	2.80	18.0%
1-88	3.80	18.0%
1-100	2.40	17.0%
1-55	2.60	15.0%
1-56	3.20	21.0%
1-58	1.30	7.0%
1-71	1.50	10.0%
1-77	1.70	11.0%
1-54	1.90	10.0%
1-67	2.50	15.0%
1-71	2.20	15.0%

3 Reservoir Simulation Model

Numerical Reservoir simulation was conducted with a commercial software package developed by ROXAR, an Emerson Process Management brand. The use of Tempest MORE in black oil mode allowed to generate synthetic hydrocarbon production for several scenarios in which relative permeability and producing bottom hole flowing pressure were evaluated above and below the bubble point

3.1 Grid Construction

3.1.1 Background on Analytical Solution

Many hydraulically fractured Bakken wells observe formation linear flow for a number of years. In 1998, Wattenbarger et al., proposed analytical solutions to determine reservoir parameters and drainage area of hydraulically fractured horizontal wells, the model, shown in Figure 17, consisted of well with a fully penetrating hydraulic fracture of infinite conductivity ($F_{CD} > 50$) located in the center of a rectangular reservoir.

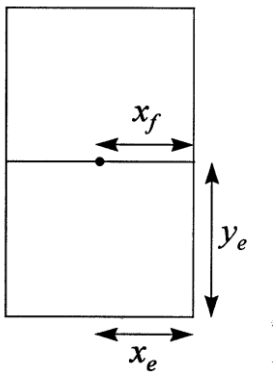

Figure 17. Model proposed by Wattenbarger (1998) for a Hydraulically Fractured well in a rectangular reservoir

Figure 18 shows a 3D view of the reservoir simulation grid based on the model proposed by Wattenbarger et al., 1998. Reservoir grid dimensions $y_{e,}, x_e$ were evaluated in relation to hydraulic fracture half length x_f to allow full observation of GOR during the duration of both transient and boundary dominated flow regimes. Grid dimensions are provided on Table 6.

Relationships between initial solution gas R_{si} and producing GOR will be presented in the results section. In order to accurately capture relative permeability changes during production, it was necessary to use local grid refinements around the hydraulic fracture. Logarithmic gridding was also used away from the fracture face to maintain run times to a minimum. Figure 19.

Table 6. Specifications used to construct simulation grid

Centre	133.0, 1329.0, 9822.5 ft
Coarse grid dimensions	38x51x1
Fine grid dimensions	38x1329x1
Num active cells	1,938
Size	266.0, 2658.0, 45.0 ft
Structure	Corner point

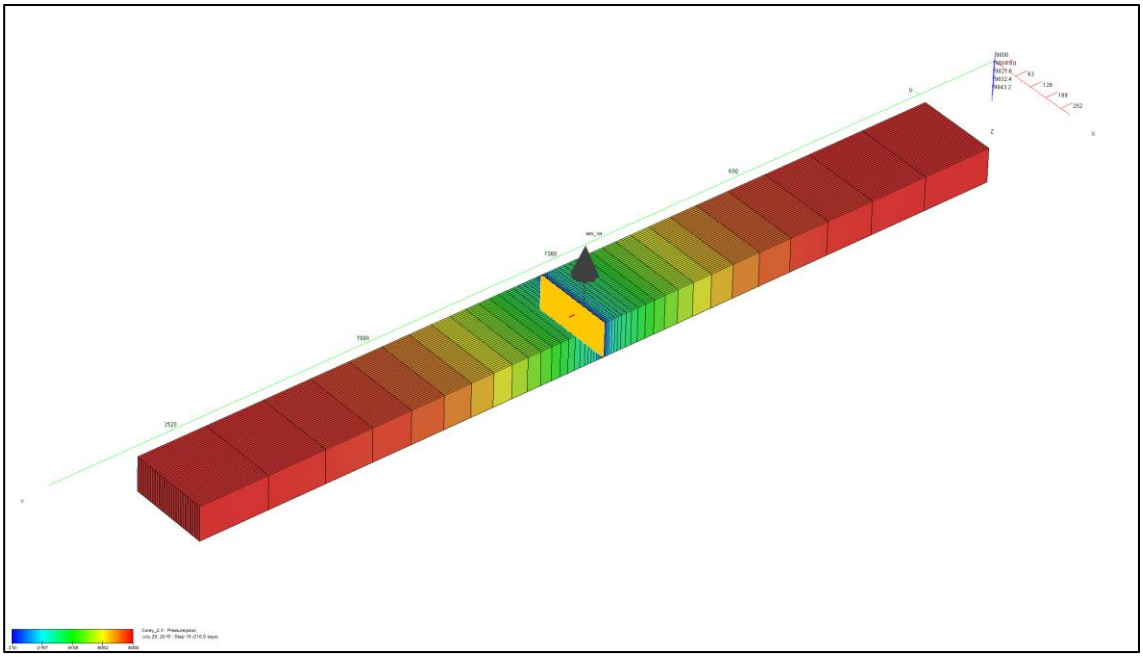

Figure 18. 3D Grid display of Reservoir Model used for Simulation. Colors indicate pore pressure transient during run time.

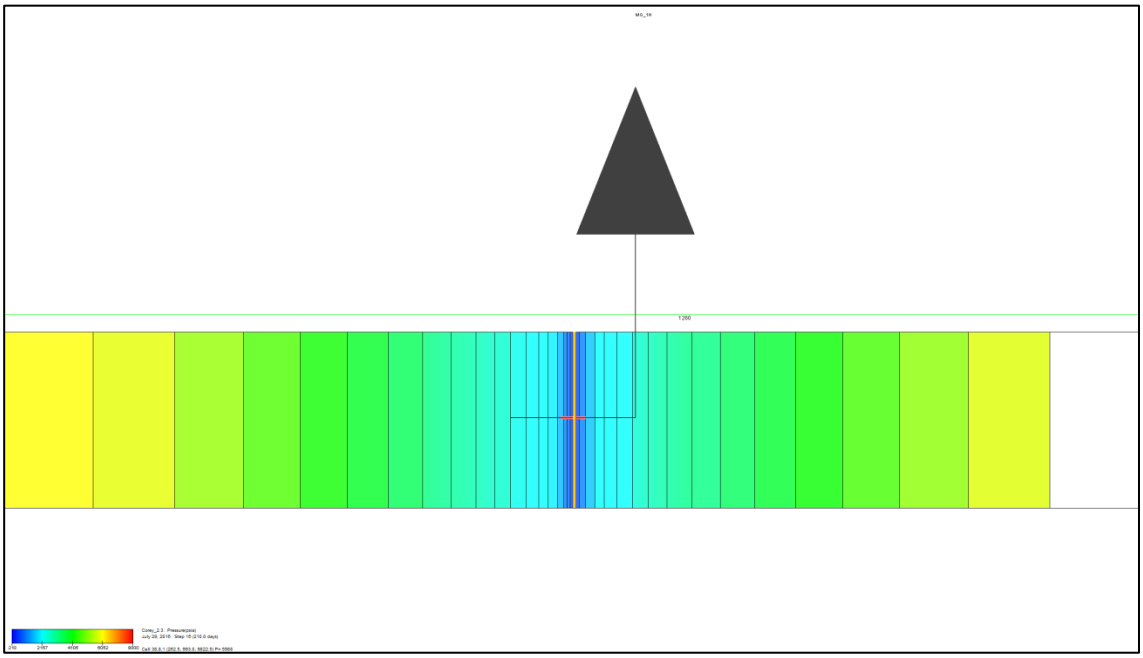

Figure 19. Side view showing a detail of simulation grid. Wellbore and Hydraulic Fracture are situated in the middle of the rectangular reservoir. Note logarithmic gridding as distance increases away from fracture face.

3.2 Reservoir and Fluid Properties

Reservoir properties used to populate the model were extracted from study wells located in McKenzie County, ND. Table 7. Full PVT analysis was available for 2 offset wells using recombined surface samples. The validity of recombination conditions was checked to ensure producing GOR was stable and flowing bottom hole pressure remained above the saturation conditions (Figure 20). Table 8 summarizes fluid properties determined experimentally that were used for the simulation model.

Figure 20. Cumulative Gas Oil Ratio vs. Producing Gas Oil Ratio during sampling time of surface sample for PVT analysis.

Table 7. Middle Bakken Reservoir Properties used for Simulation

P_i [psi]	8,000
P_{wf} [psi]	6000, 200
BHST [^oF]	264
S_o [%]	65
k [md]	0.01
ϕ [%]	6.5
x_f [ft]	133
$k.x_f$ [md.ft]	500

Table 8. PVT fluid properties used for simulation

B_{oi} [res bbl/stb]	1.898
C_{oi} [(V/V/psi) x 10^{-6}]	14.40
μ_o[cP]	0.175
API	43.60
P_b [psi]	3,130
R_{si} [scf/bbl]	1,638
γ_g (76 psi, 124 ^oF)	0.9772

3.3 Relative Permeability Curves

Figure 16 provided a distribution of wetting phase exponents n_o found thru matching of experimental data. However we note that in equation 14 when $n_o < 2$, S_{oe} is raised to a negative exponent and the term $(1 - S_{oe}^{(n_o-2)})$ becomes negative, additionally if $n_o = 2$ equation 14 becomes equal to zero or K_{rg}will incorrectly be assumed to take a null value.

Given this constraint, when using the Corey-Brooks model, n_o values are limited to $2 < n_o < 3.8$. Figure 21 displays the new constrained distribution and Figure 22 presents the relative permeability curves used for simulation derived from using values of $n_o = 2.3, 2.7, 3.2, 3.8$.

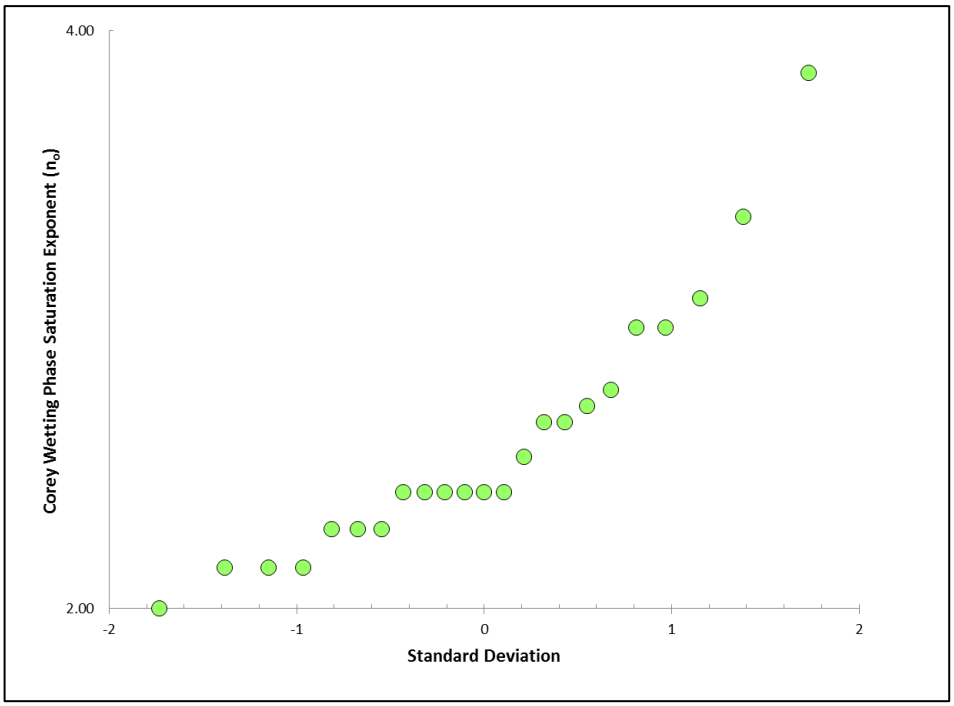

Figure 21. Wetting Phase exponent distribution for values $n_o > 2$

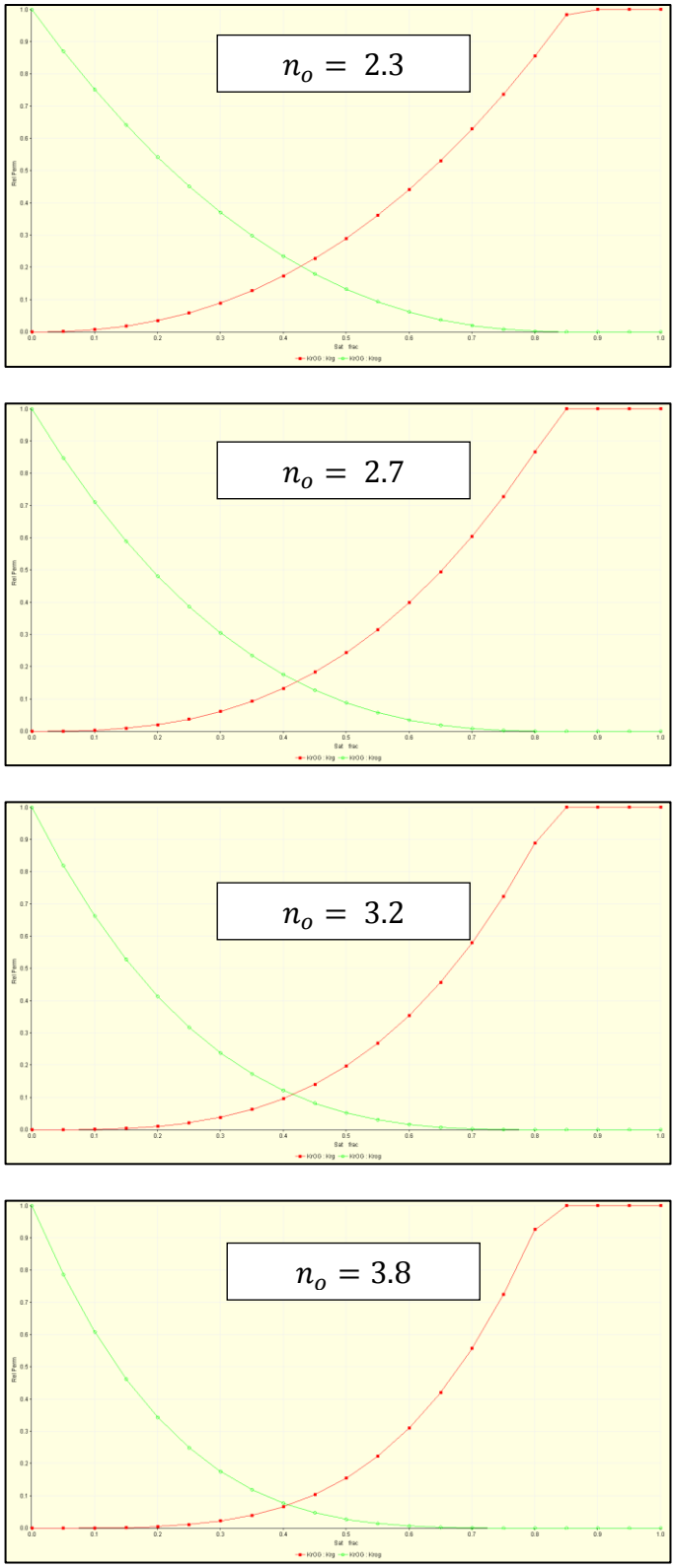

Figure 22. Gas-Oil Relative Permeability Curves used for Simulation.

3.4 Simulation Output

Synthetic production data was generated using the reservoir simulator. Two runs were conducted for each one of the wetting phase saturation exponents. An initial run was conducted above the saturation pressure P_b using a bottom hole flowing pressure P_{wf} of 6,000 psi. As gas never evolves from the system this run is unique an independent of any wetting phase exponent value. This is shown on Figure 23 when comparing outputs from $n_o = 2.3$ and $n_o = 2.7$.

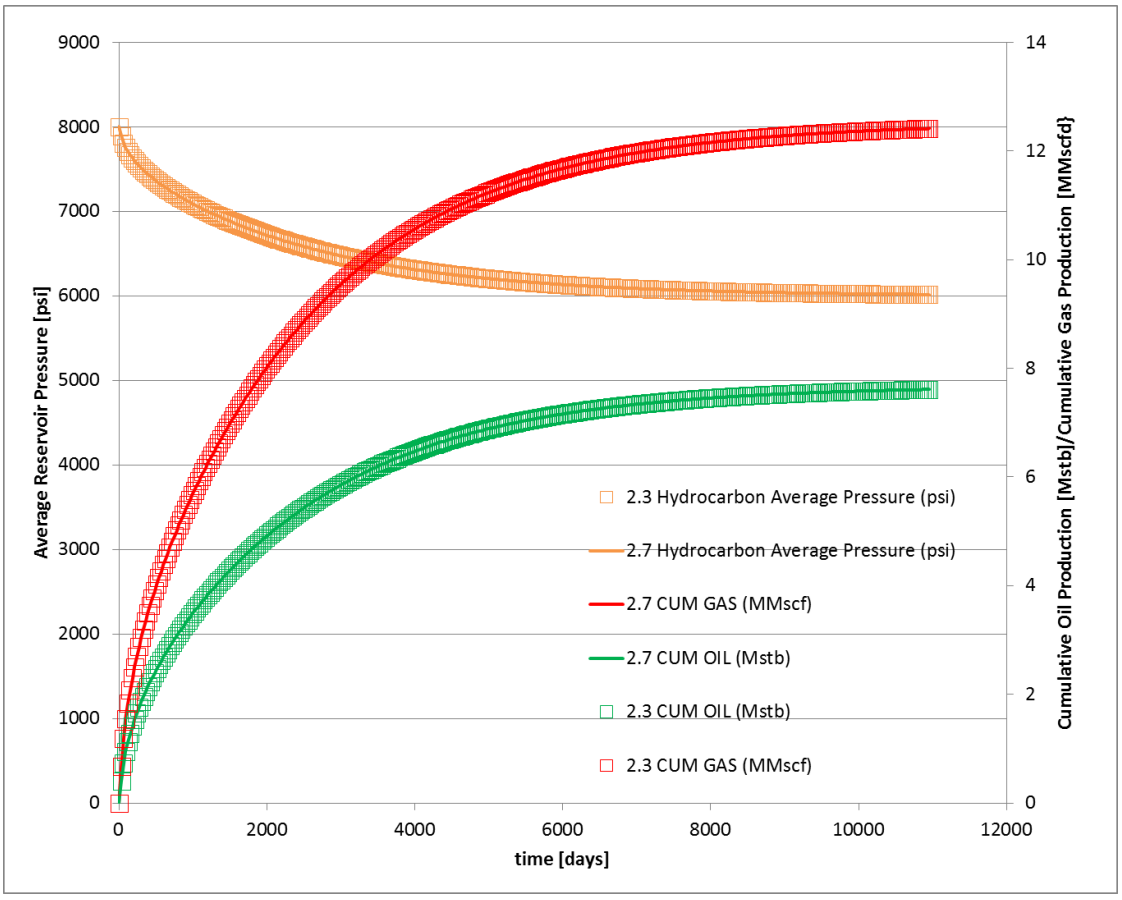

Figure 23. Reservoir simulator output for case 0. Production rates are independent of n_o values when $P_{wf} = 6000\ psi$ is above bubble point.

Table 9 provides cumulative hydrocarbon production for each one of the runs after a simulation time of 30 years.

Table 9. Synthetic Cumulative Hydrocarbon Production for all runs studied.

	n_o	P_{wf} [psi]	G_p [MMscf]	N_p [Mstb]
case 0	all	6,000	12.41	7.611
case 1	2.3	200	70.79	35.03
case 2	2.7	200	75.59	32.24
case 3	3.2	200	77.65	29.69
case 4	3.8	200	78.30	27.41

4 Production History Matches

4.1 Specialized Plots

Linear flow can be diagnosed by plotting reciprocal rate $1/q$ vs. square root of time $\sqrt{t}$ plot. The solution, originally proposed in 1998 by Wattenbarger was applied to gas reservoirs, however it has been expanded later to oil reservoirs and it has been used successfully diagnosing linear flow in the Bakken (Gonzales, 2011) and the Eagle ford (Rodrigues, 2012).

The solution, based on a constant pressure case allowed determination of linear flow and the calculation of reservoir properties from the observed slope

$$m_{rrc}{}^{0.5} = \frac{31.28 B_o \mu}{h\sqrt{\phi(\mu c_t)_{Pfp}}} \frac{1}{\Delta P \sqrt{k} x_f} \qquad (15)$$

Figure 24 presents a reciprocal rate vs. square root of time plot of synthetic production generated by the simulation of case 3. Similar plots were also constructed for all other cases indicated in Table 9 but those are not presented here.

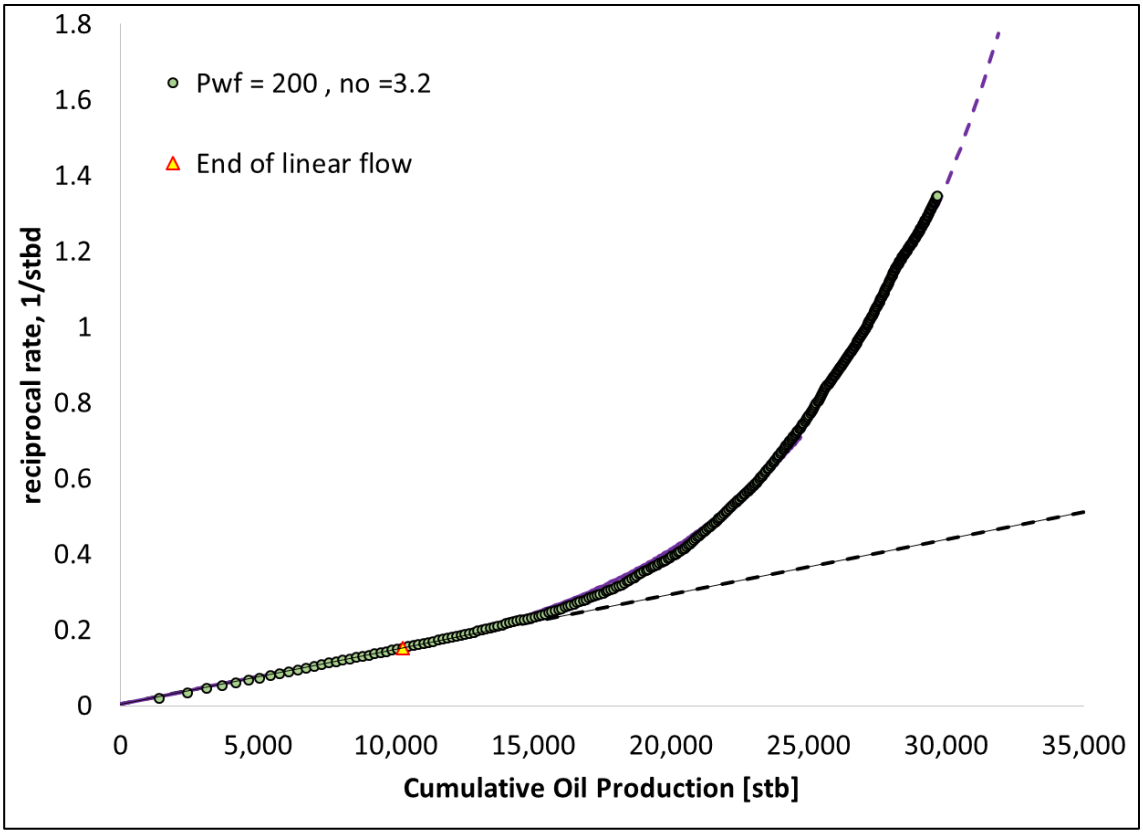

Figure 24. Reciprocal rate vs Cum Production plot for case 3.
($n_o = 3.2\ P_{wf} = 200\ psi$)

Rodriquez and Callard, 2012, also proposed the use of a cumulative production – square root time plot in cases where the reciprocal rate data was noisy or production did not fully meet the constant pressure requirement. Figure 25 displays an example of such plot for case 3. The time to end of linear flow t_{elf} could be estimated from the deviation of the straight line and calculated as:

$$t_{elf} = \frac{m_{rrc}}{2} {N_{pelf}}^2 + \frac{1}{q_i} N_{pelf} \qquad (16)$$

where m_{rrc} is the slope during the linear flow regime in a reciprocal rate and cumulative production.

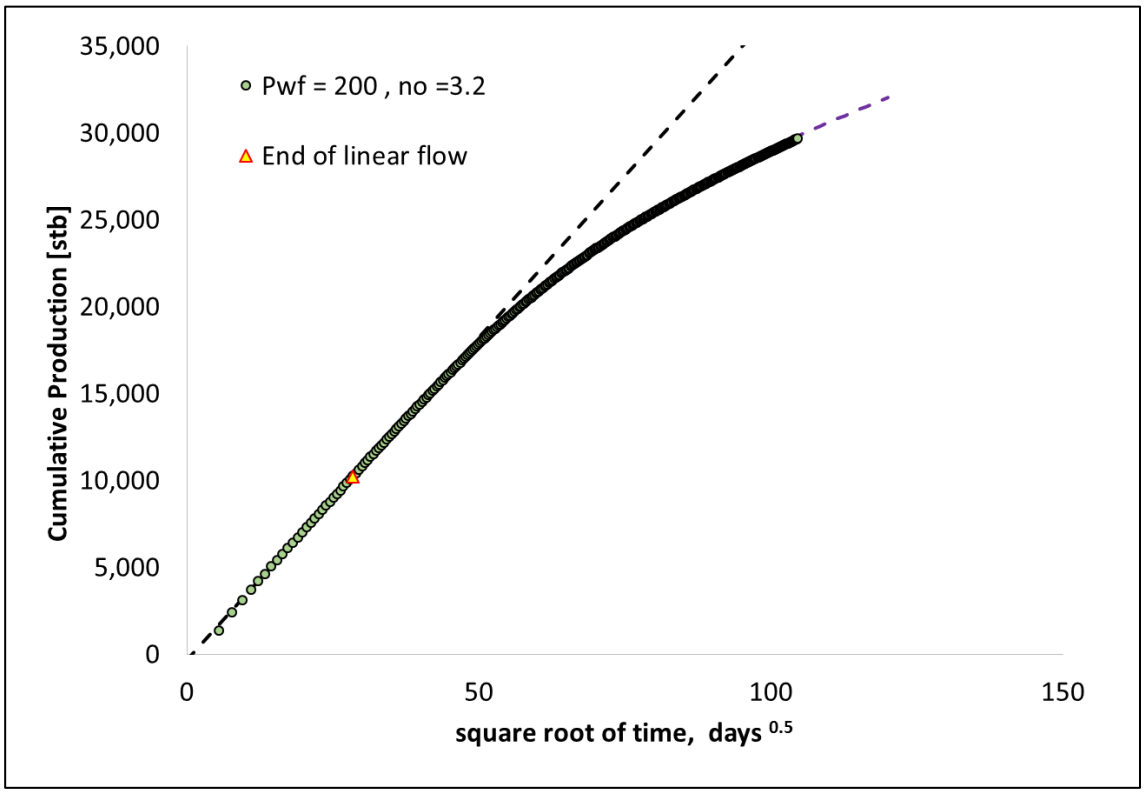

Figure 25. Plot of Cumulative Production vs. Square root of time for case 3. ($n_o = 3.2$ $P_{wf} = 200$ psi)

4.2 Type Curves

The reciprocal rate and cumulative production variables are related by the hyperbolic form of Arp's equation for a b exponent of 2 (Arps, 1956), this allows cumulative production time relationships to be used for linear flow determination, on this basis, Khan and Callard, 2010 developed a rate-cumulative relation which was employed in conjunction with a value of m_{cp} to generate the following expression:

$$N_p = \frac{2}{m_{cp}}\sqrt{t} \tag{17}$$

With a determination of the time to end of linear flow t_{elf} and the corresponding cumulative production N_{pelf}, we can normalize equation 17 for differences in the fracture geometry and the reservoir properties defined in the analytical solutions. Figure 26 presents the cumulative production ratio – square root time ratio plot developed to conduct the production matching with field data.

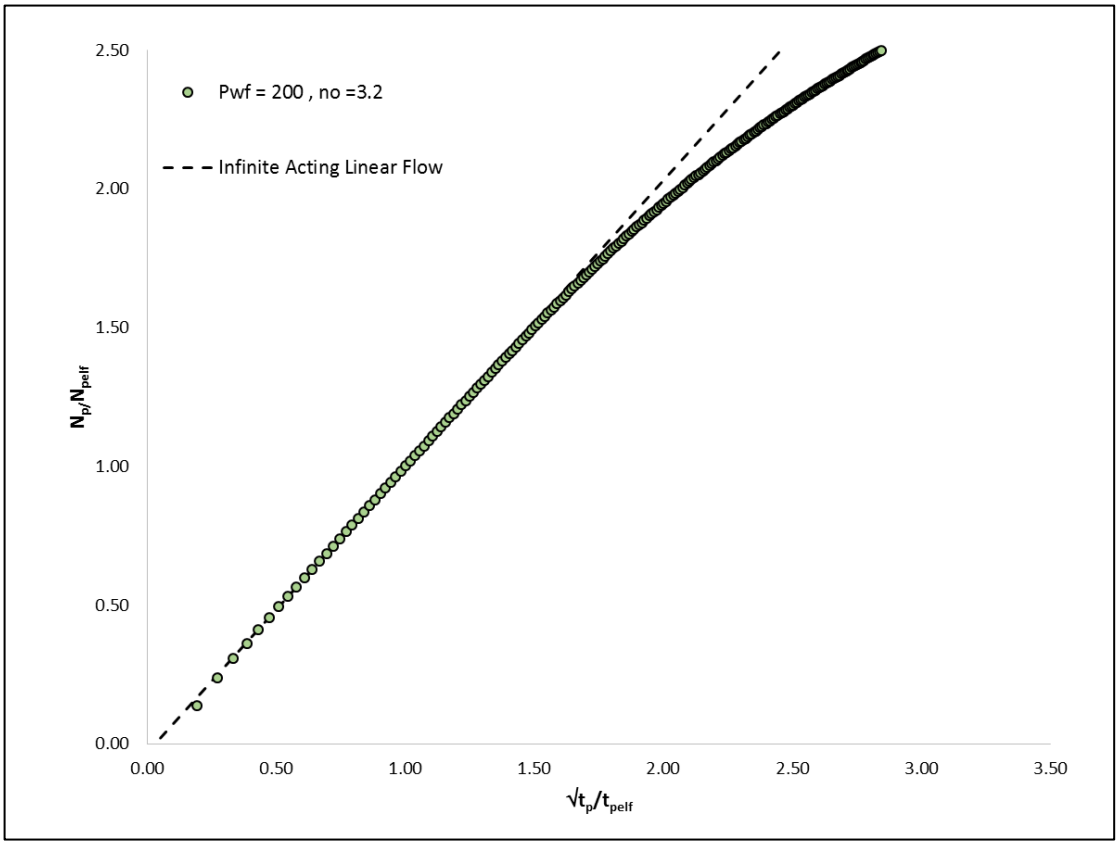

Figure 26. Plot of Cumulative Production ratio vs. Square root of time ratio for case 3. ($n_o = 3.2$ $P_{wf} = 200$ psi)

4.3 Matching Field Data to Type Curves

In order to relate simulation output with field production, a family of type curves was created using the cumulative production ratio – square root time ratio plot for the study of all wetting phase saturation exponent cases. Figure 27.

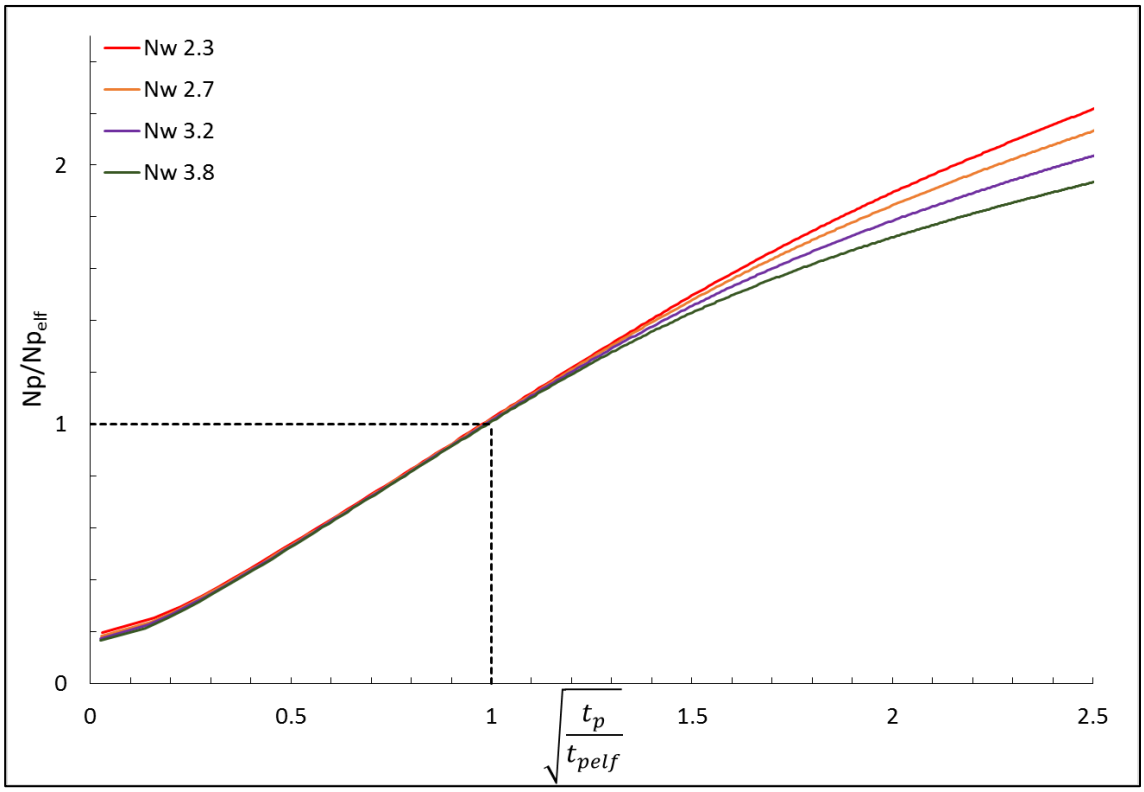

Figure 27. Type curve developed for Bakken study cases.

Using specialized plots t_{elf} and the corresponding cumulative production N_{pelf} was determined for the study wells. As previously explained, end of linear flow will be detected by a departure of the straight line behavior. A verification of the value of t_{elf} selected for the analysis can be achieved by the simultaneous departure from linear flow observed on both specialized plots.

An example of the production analysis conducted on the well ANSETH 1-29H is shown in Figures 28 and 29.

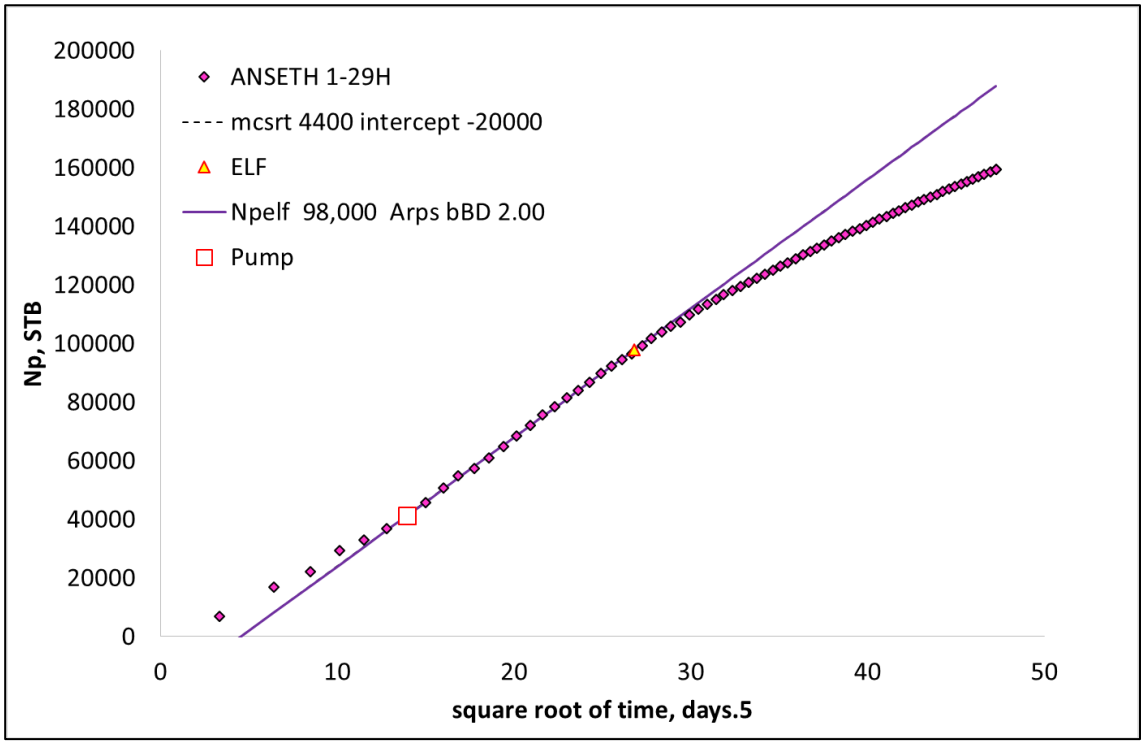

Figure 28. ANSETH 1-29H. Determination of t_{elf} via Cumulative Production vs. Square root Time plot

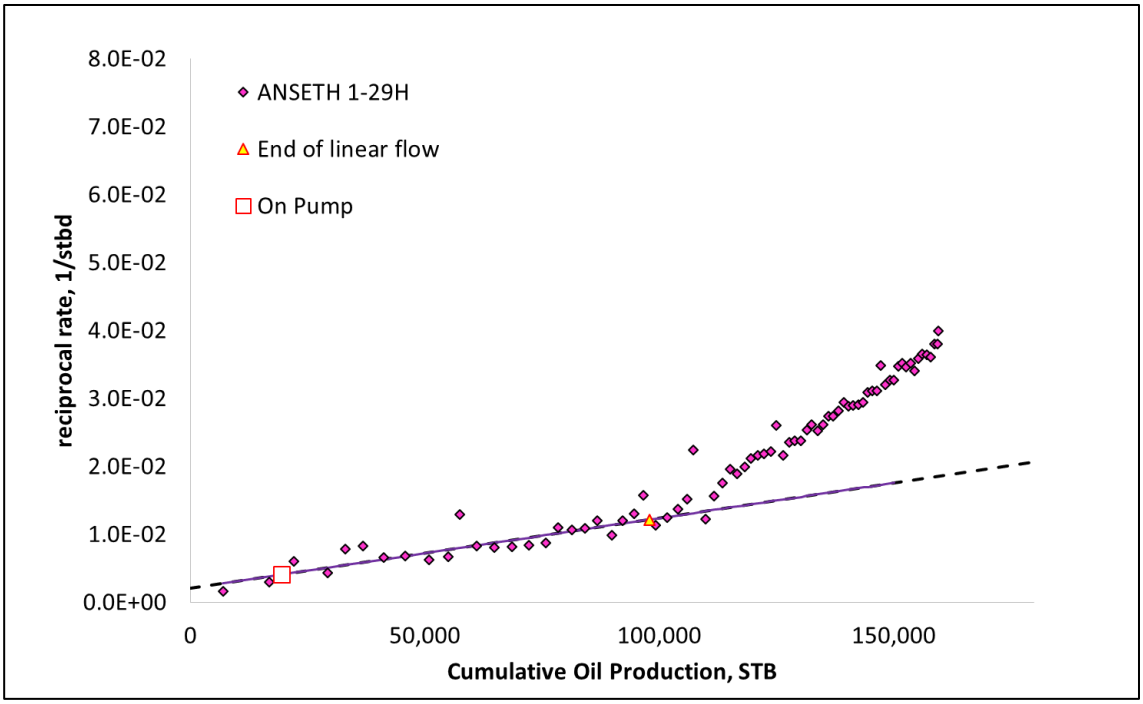

Figure 29. ANSETH 1-29H. Determination of t_{elf} via Reciprocal Rate vs. Cumulative Production

With the determination of both t_{elf} and N_{pelf} from the specialized plots, field production can be normalized and plotted over the type curve. A match of filed observed values with the simulated generated type curve implies that the particular wetting phase exponent value for that curve can be used to describe the relative permeability behavior of such well. Figure 30 and 31 provides examples for the matches achieved on wells ANSETH 1-29H and PANASUK 1-23H , with values of $n_o = 3.8$ and $n_o = 2.3$ respectively.

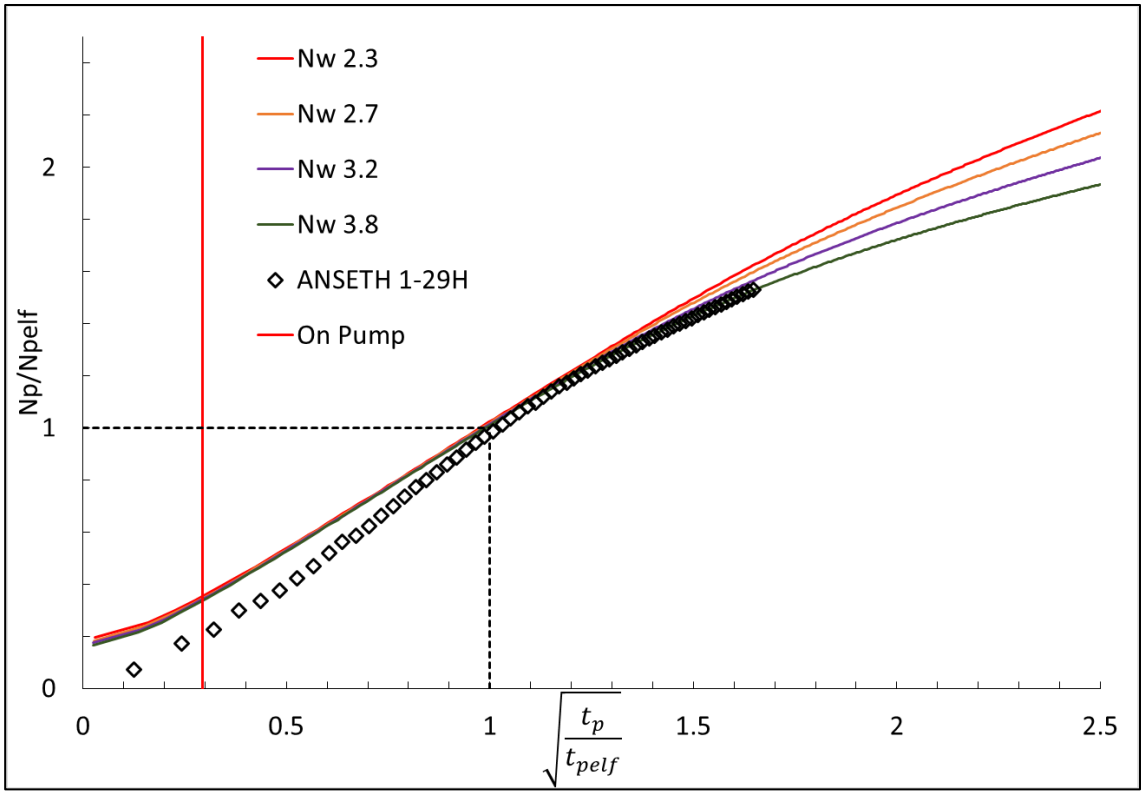

Figure 30. ANSETH 1-29H Oil Production analysis indicating a match with a wetting phase exponent of 3.8

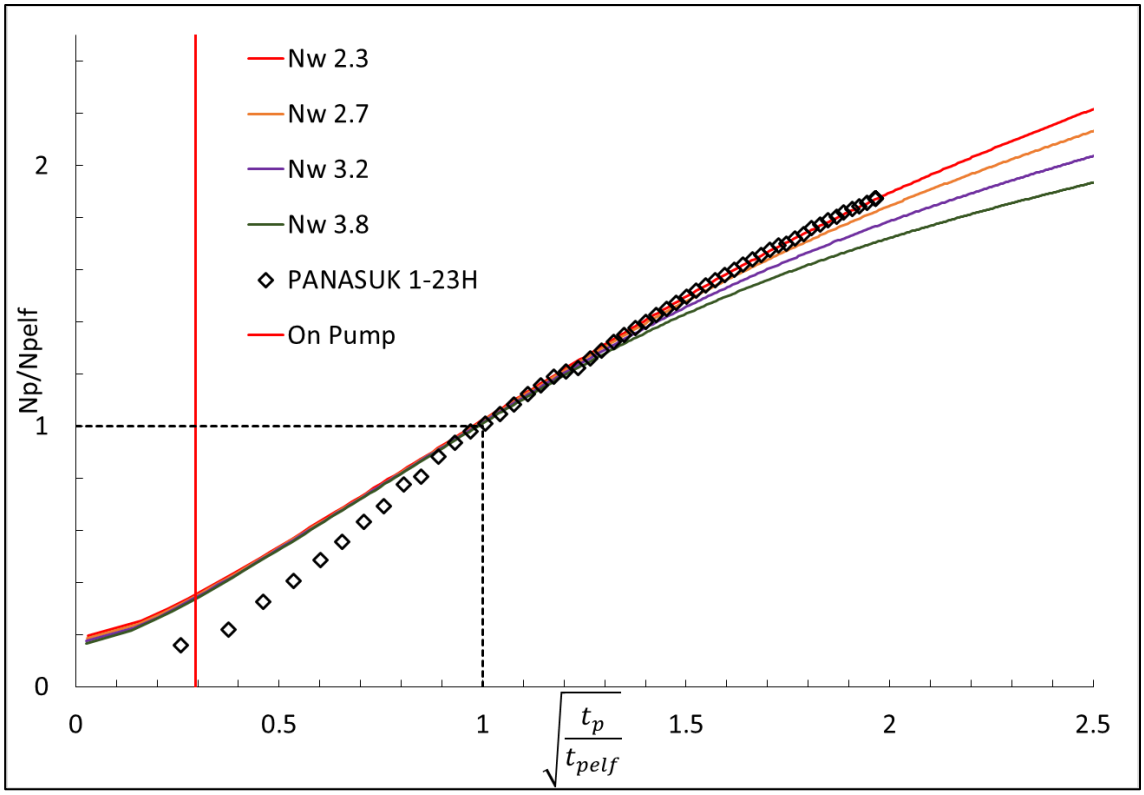

Figure 31. PANASUK 1-23H Oil Production analysis indicating a match with a wetting phase exponent of 2.3

4.3.1 Effects of Pump Installation Time

Middle Bakken wells typically require artificial lift within the early years of production. The most common method of artificial lift is the use of a downhole rod operated pump. Identifying the time in which the well goes on pump (pump installation time) greatly improves the accuracy of determination of time to end of linear flow t_{elf}. It has been observed a difference in the behavior of field production before and after the pump installation time. This behavior is more easily detected when data is evaluated over the cumulative time- square root of time plot.

Figure 32 below provides an example of what is often seen during the analysis of field data. Four distinct periods can be readily identifiable:

Variable Pressure: Early time flowing data is typically associated with constant changes in choke size typically due to operators attempting to increase hydrocarbon production rates at the expense of higher drawdowns. During this period of time bottom hole pressure falls rapidly from its initial values. The opinion of the author is that the noise in the data is due to the lack of accuracy analytical solution to capture variable pressure.

Stabilization Period: After the well quits flowing and a rod pump is installed, fluid level is typically high and the drawdown is now controlled by the pump capacity to pump the fluid level down "pump-off condition".

Pseudo constant Pressure: System behaves as if the bottom hole pressure was constant. This is again controlled by pump efficiency and size. During this period of time, the analytical solution for the constant pressure case is able to model the good behavior with little deviation. Infinite acting linear flow is easily detected and a values for the slope m_{cp}can be calculated.

Boundary Dominated Flow: The onset of boundary dominated flow is detected and t_{elf} value can be found.

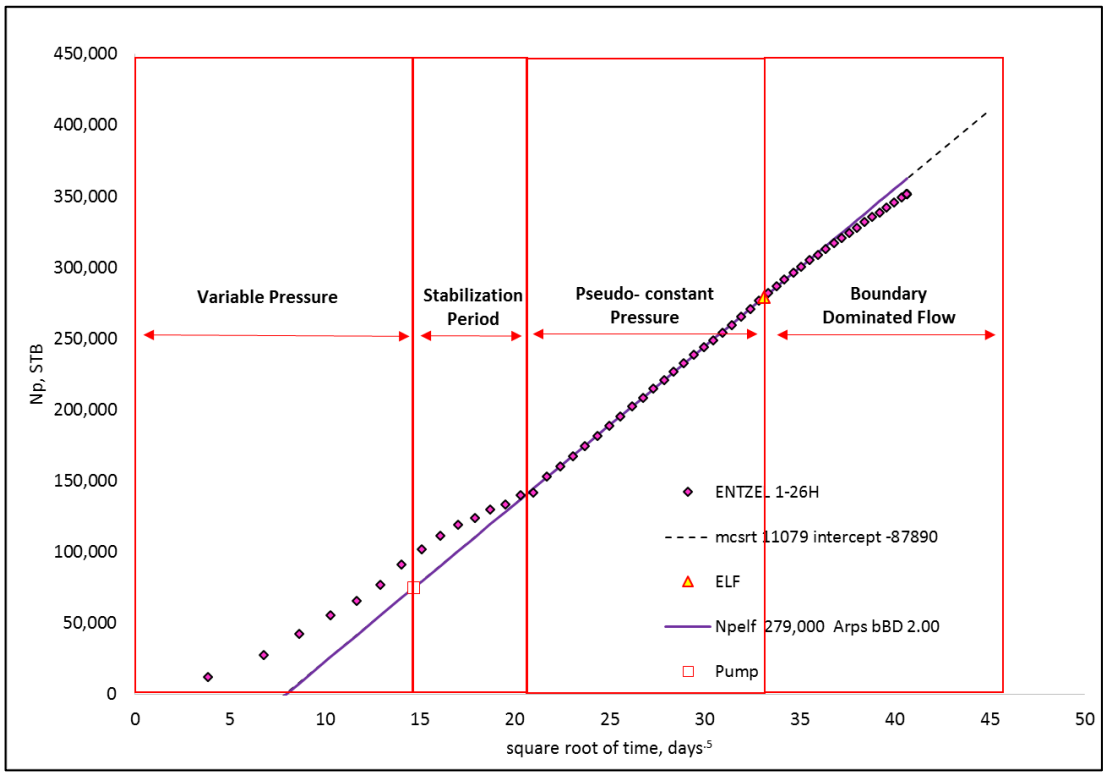

Figure 32. ENTZEL 1-26H. Indicating typical behavior seen after pump installation time.

5 Results and Other Findings

Figure 33 indicates the surface location of Middle Bakken wells used for production matching. Monthly production data available from the North Dakota Industrial Commission (NDIC) was required to populate the specialized plots. Table 10, summarizes n_o derived from the application of type curves to field production.

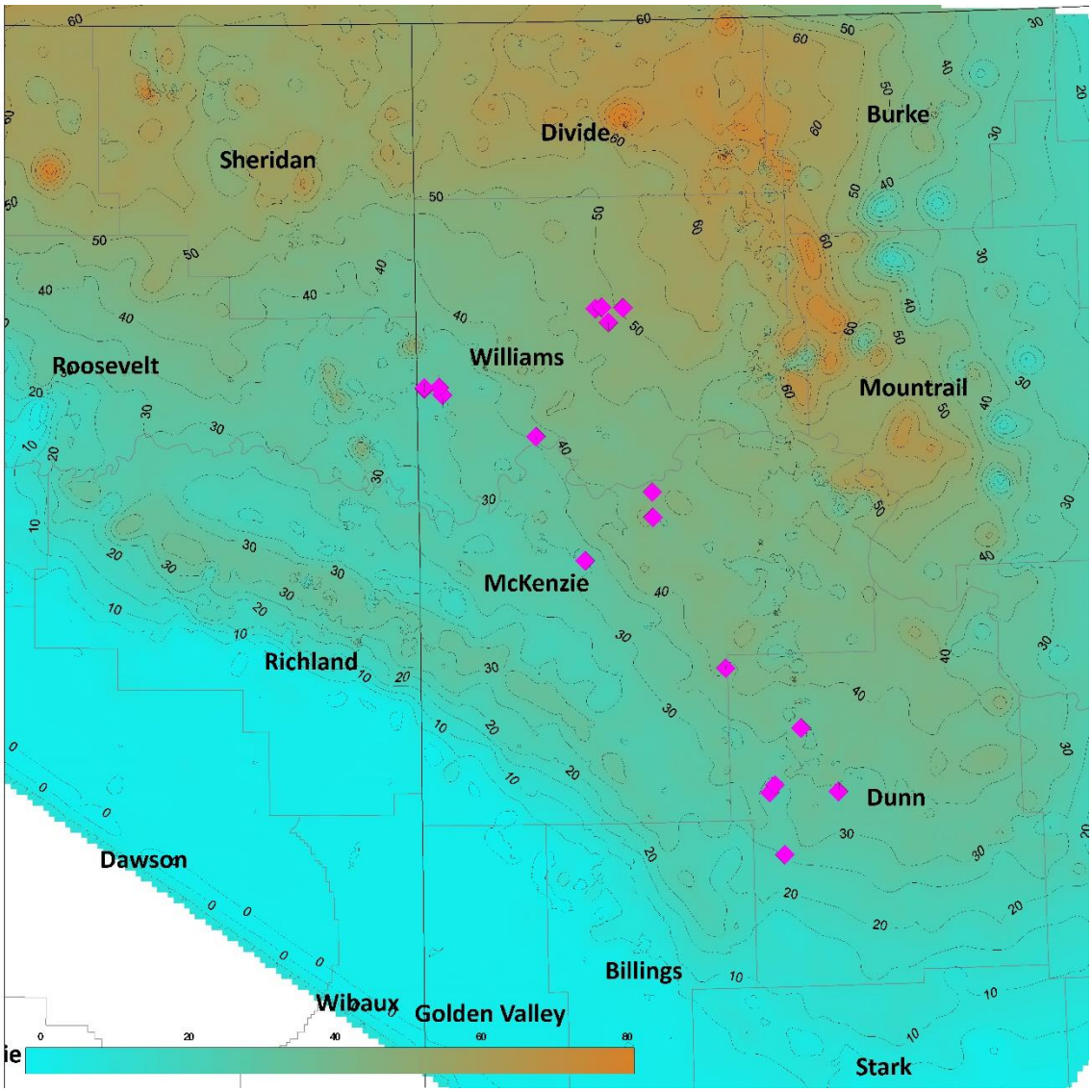

Figure 33. Location of Middle Bakken wells selected for Production Analysis.

Table 10. Summary of wetting phase saturation exponents found thru Production Analysis.

Well Name	n_o	Field	County	State	1st Production Date	N_p at pump time	N_{pelf}
ANSETH 1-29H	**3.8**	SQUIRES	WILLIAMS	ND	05/2010	19,524	86,000
BENNER 1-6H	**2.3**	JIM CREEK	DUNN	ND	01/2012	60,993	123,000
BERLAIN 1-30H	**2.3**	PATENT GATE	MCKENZIE	ND	12/2011	72,056	117,000
CLOVER 2-10H	**2.6**	MURPHY CREEK	DUNN	ND	07/2012	90,500	200,000
ENTZEL 1-26H	**2.3**	CABERNET	DUNN	ND	12/2011	75,000	279,000
FELLER 1-22H	**2.3**	LONE TREE LAKE	WILLIAMS	ND	05/2012	23,148	60,000
HOROB 1-14H	**2.7**	HEBRON	WILLIAMS	ND	01/2011	20,073	95,000
INGA 2-12H	**3.8**	HAYSTACK BUTTE	MCKENZIE	ND	08/2011	131,802	170,000
MARSHALL 1-13H	**2.3**	LITTLE KNIFE	DUNN	ND	07/2011	48,700	85,000
MATHEWSON 1-30H	**2.3**	OLIVER	WILLIAMS	ND	04/2012	42,430	110,000
MONROE 1-2H	**2.7**	BANKS	MCKENZIE	ND	08/2012	157,859	180,000
MORRIS 3-26H	**2.7**	OAKDALE	DUNN	ND	05/2011	241,250	252,000
PANASUK 1-23H	**2.3**	HEBRON	WILLIAMS	ND	09/2010	13,047	60,000
PLANO 1-28H	**2.3**	TODD	WILLIAMS	ND	03/2012	57,632	137,000
RICKY 1-18H	**2.4**	SQUIRES	WILLIAMS	ND	07/2010	16,596	63,000
RIXEY 1-28H	**3.2**	LONE TREE LAKE	WILLIAMS	ND	03/2012	89,982	122,000
SEAVER 1-5H	**2.5**	EAST FORK	WILLIAMS	ND	06/2012	34,063	87,000
SYRACUSE 1-23H	**3.2**	BANKS	MCKENZIE	ND	06/2011	220,969	229,000

Figure 34 presents a comparison of the relative permeability distributions derived from laboratory and the relative permeability distributions from production analysis. Examination of both distributions reveals that both the ranges of values and a median of the distributions seem to agree even when the methodology used to generate the values greatly differs.

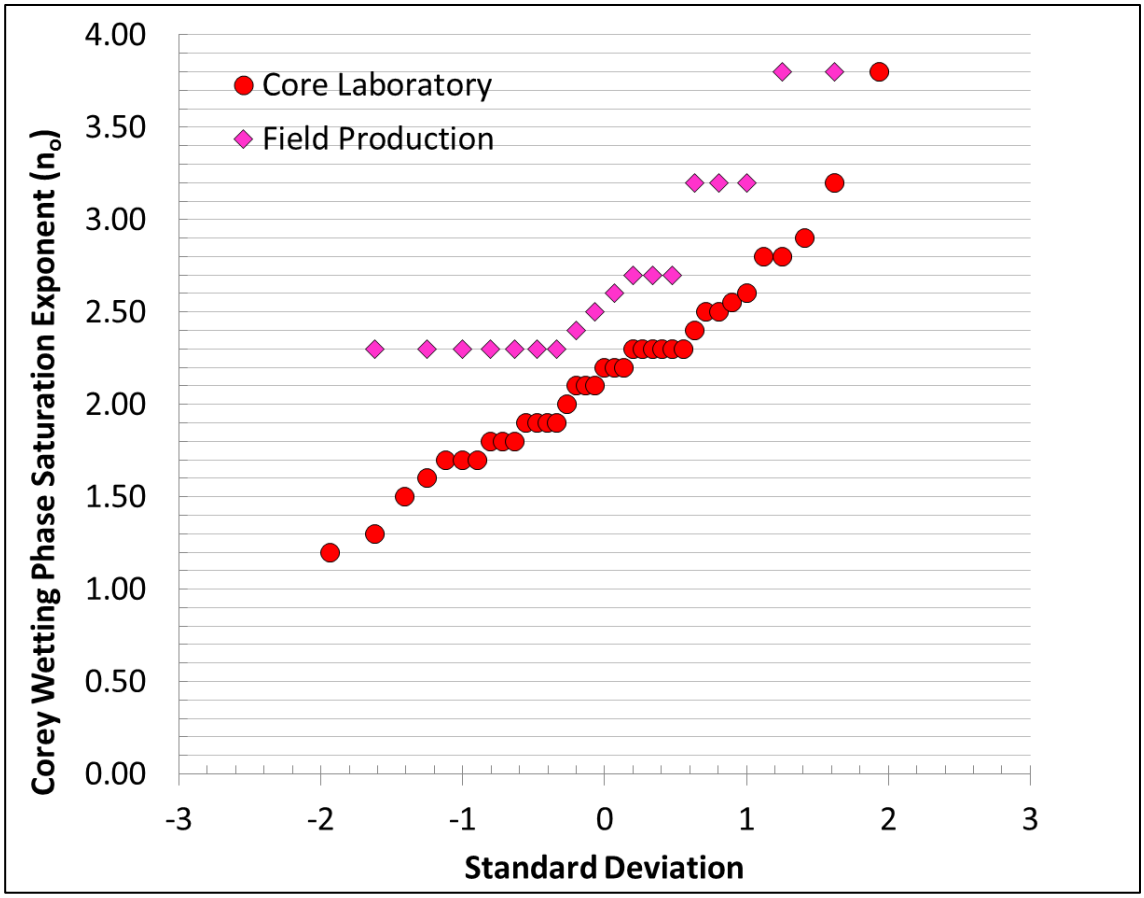

Figure 34. Comparison of the relative permeability distributions derived from laboratory and the relative permeability distributions from production analysis.

5.1 Additional Findings

5.1.1 Gas Oil Ratio Observations

Previous authors have indicated that an examination of *GOR* behavior aids in the interpretation of both infinite acting and boundary dominated flow (Gonzales, 2011). The theoretical behavior of *GOR* in our model is indicated in Figure 35. During initial production, *GOR* is equal to the initial gas solubility R_{si}, after reaching the bubble point pressure and exceeding the critical gas saturation an elevated but yet constant new value of *GOR* is observed during the linear flow period GOR_{LF}.

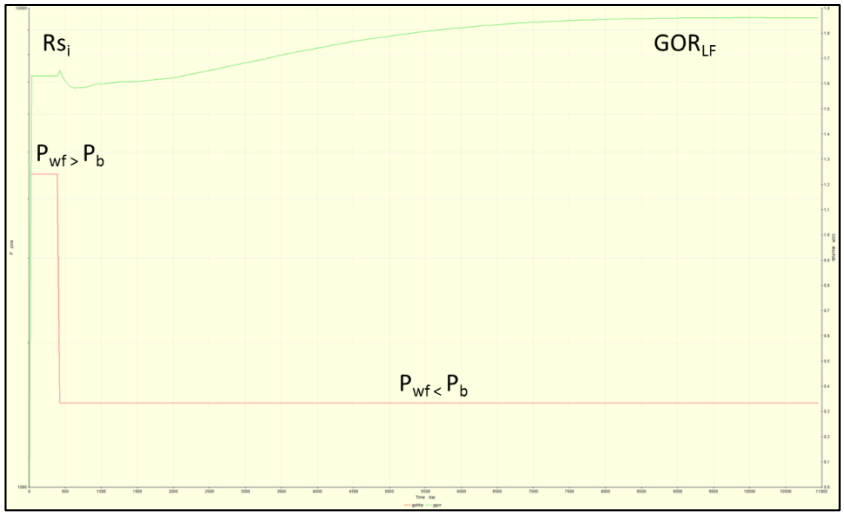

Figure 35. Reservoir Model *GOR* theoretical behavior

This *GOR* behavior can be also observed when plotting the cumulative *GOR* (R_p) vs. the cumulative oil production N_p. The onset of boundary dominated flow is indicated by the inflection in both R_p and the reciprocal rate curve as shown in Figure 36.

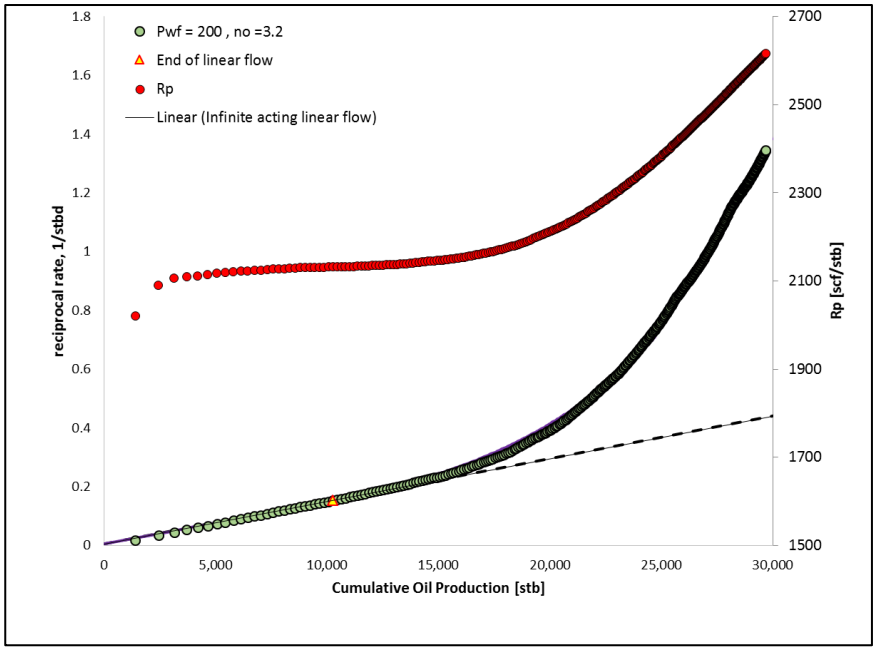

Figure 36. Elevation of Cumulative GOR observed at the onset of boundary dominated plot.

Output values of *GOR* for simulation runs were analyzed and normalized by the original gas solubility R_{si}. Elevation ratios $\frac{GOR_{LF}}{R_{si}}$ were calculated for each one of the cases as indicated on Table 11. These ratios were used to create a second type curve in which field data could be evaluated and matched.

Table 11. Elevation ratios calculated from simulation Runs

	n_o	P_{wf}	GOR_{LF}	GOR_{LF}/R_{si}
case 1	all	6,000	1,631	1.00
case 2	2.3	200	1,822	1.12
case 3	2.7	200	2,014	1.23
case 4	3.2	200	2,145	1.32
case 5	3.8	200	2,243	1.38

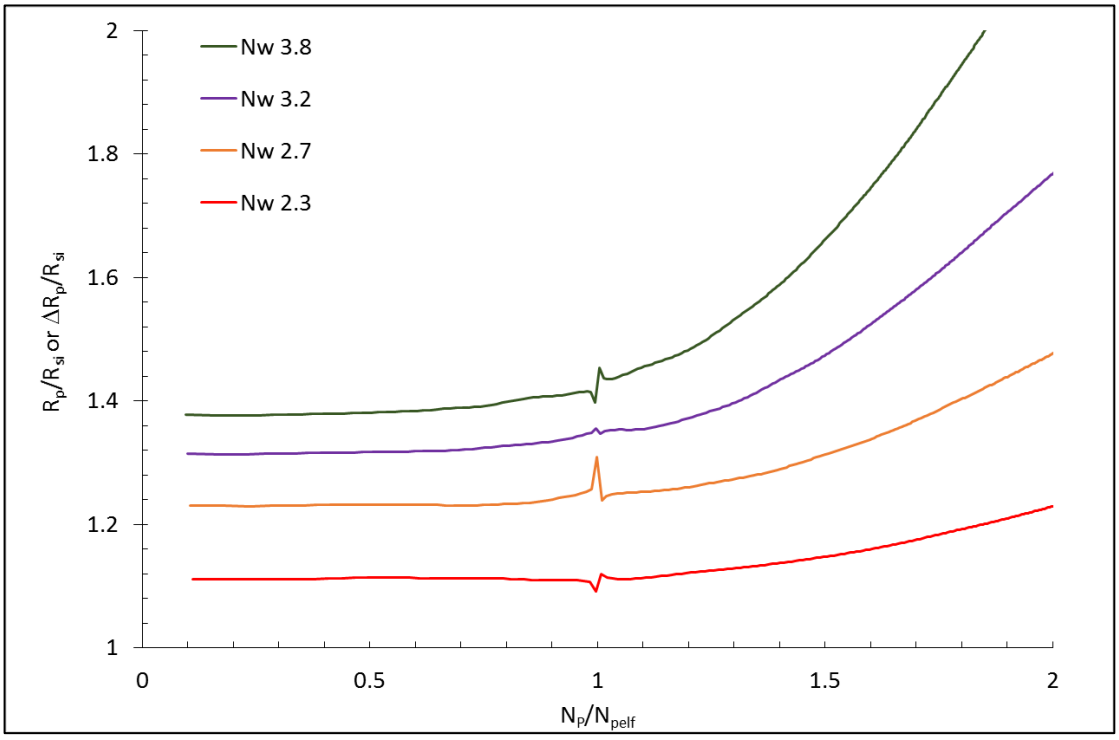

Figure 37. Type curves developed from elevated Cumulative Gas-Oil Ratio

5.1.2 Application to Field Production

Our research has revealed that the application of this technique in the Bakken is limited to wells in which there is high confidence in the gas measurement. It is the opinion of the author that noise observed in the field data is due to incorrect reporting of natural gas production mainly due to flaring or not calibrated gas meters. The EIA reports that the percentage of gas not marketed in North Dakota increased an additional 15% between 2010 and 2012. Figure 38. Unfortunately, as shown in Table 10 our study cases had first production dates that felt within this range.

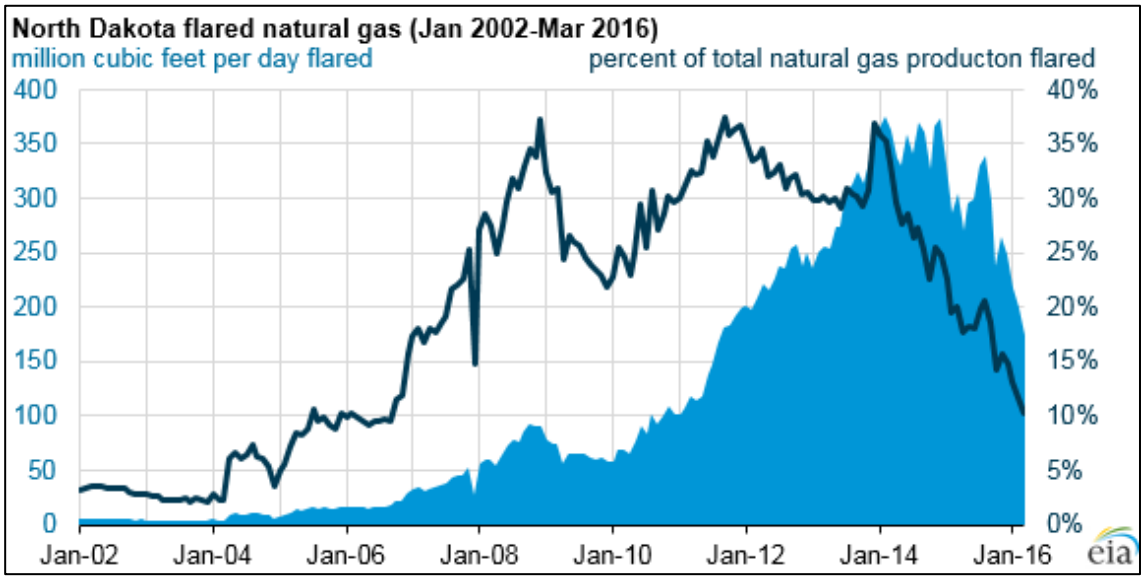

Figure 38. Percent of natural gas flared in North Dakota.

5.1.3 Case Study

An example of the application of this technique is presented for well ENTZEL 1-26H. Determination of time and cumulative oil production to end of linear flow is performed with the specialized plots as explained in section 4.1. Figure 31 provides a

cumulative production – square root time plot. An additional solution was proposed in order to normalize the cumulative gas oil ratio after the onset of boundary dominated flow. The following relationship allowed matching the type curve stem after N_{pelf} is reached.

$$R_p = \frac{(G_p - G_{pelf})}{(N_p - N_{pelf})}.1000 \qquad (18)$$

where $G_{pelf} = N_{pelf}.GOR_{LF}.1000$

Using the above solution we can lay field production values over the type curve and obtain a match. Figure 39.

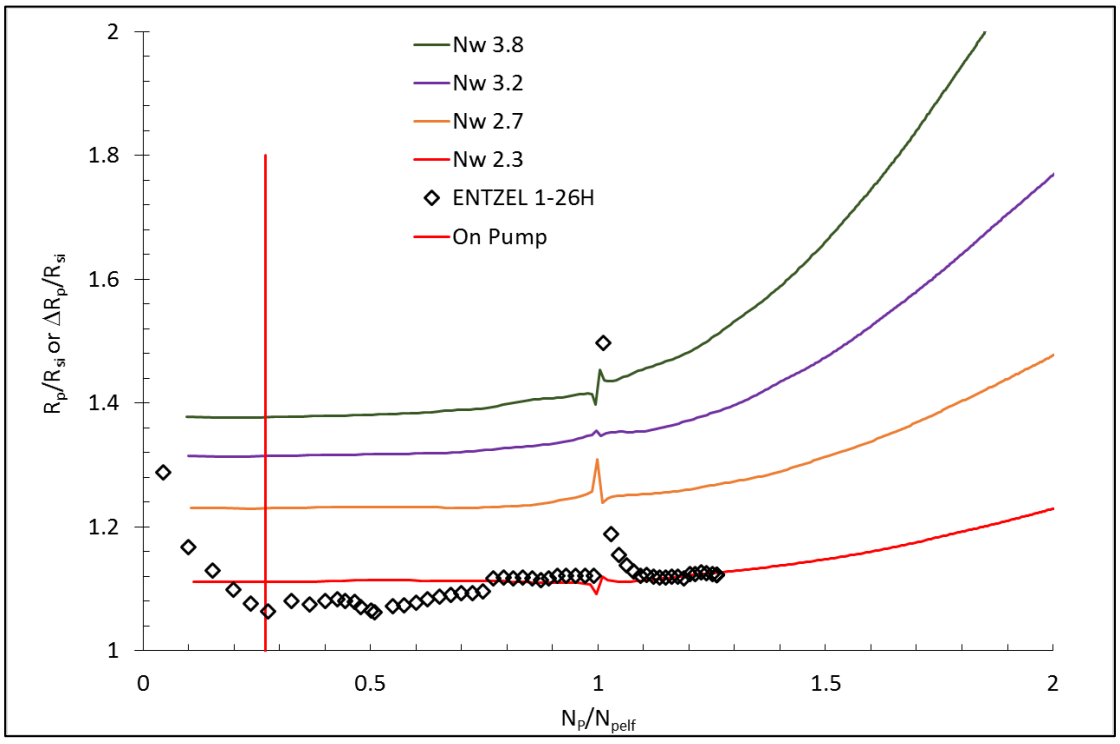

Figure 39. ENTZEL 1-26H. Oil Production analysis indicating a match with a wetting phase exponent of 2.3

5.2 Conclusions

- The median of wetting phase saturation exponents for the Middle Bakken formation ranges between values of 2.3-2.6.
- Corey exponents derived from the application of type curve to field production have a narrower distribution due to limitations of the model.
- A new type curve has been developed in which oil production and transition from linear to boundary dominated flow are the two requirements needed to derive oil-gas relative permeability.
- Observation of elevated Gas Oil Ratio can aid in the interpretation of well performance and improve predictive models for reserve projections using normalized GOR type curves.

5.3 Recommendations and Future Work

This research provides an opportunity to obtain robust relationships between production and relative permeability by simultaneously matching field production with the determination of normalized cumulative oil production during linear flow and corresponding elevated GOR ratios at the onset of boundary dominated flow.
The recommendation is to apply the production analysis techniques to an additional set of wells in which both gas and oil rates have been carefully monitored.

A similar workflow can be applied to laboratory core analysis of Three Forks samples to test the validity of the relationships to additional reservoirs within the Bakken Petroleum system.

The generation of maps of wetting saturation exponents could potentially reveal relationships with other petrophysical parameter and aid in understanding regional or spatial trends for future development.

References

1. Alharthy, N. S., Nguyen, T., Teklu, T., Kazemi, H., & Graves, R. (2013, September 30). Multiphase Compositional Modeling in Small-Scale Pores of Unconventional Shale Reservoirs. Society of Petroleum Engineers. doi:10.2118/166306-MS
2. Arps, J.J. "Estimation of Primary Oil Reserves." AIME Transactions. 207. (1956): pp. 182-91.
3. Bailey, S. 2009. Closure and Compressibility Corrections to Capillary Pressure Data in Shales. DWLS Workshop presented 19 October 2009, Golden, Colorado.
4. Behrenbruch, P., & Goda, H. M. (2006, January 1). Two-Phase Relative Permeability Prediction: A Comparison of the Modified Brooks-Corey Methodology with a New Carman-Kozeny Based Flow Formulation. Society of Petroleum Engineers. doi:10.2118/101150-MS
5. Brooks, R.H., and Corey, A.T., (June 1966). Properties of Porous Media affecting fluid flow, Journal of Irrigation and Drainage Division.
6. Brooks, R.H., and Corey, A.T., 1964, Hydraulic properties of porous media: Hydrology Papers, Colorado State University, Colorado.
7. Comisky, J. T., Newsham, K., Rushing, J. A., & Blasingame, T. A. (2007, January 1). A Comparative Study of Capillary-Pressure-Based Empirical Models for Estimating Absolute Permeability in Tight Gas Sands. Society of Petroleum Engineers. doi:10.2118/110050-MS
8. Fatt, I., & Dykstra, H. (1951, September 1). Relative Permeability Studies. Society of Petroleum Engineers. doi:10.2118/951249-G

9. Gonzales, V. M., & Callard, J. G. (2011, January 1). Optimizing Horizontal Stimulation Design Utilizing Reservoir Characterization from Decline Curve Analysis. Society of Petroleum Engineers. doi:10.2118/142382-MS
10. Gupta, R., & Maloney, D. R. (2014, November 10). Intercept Method - A Novel Technique to Correct Steady-State Relative Permeability Data for Capillary End-Effects. Society of Petroleum Engineers. doi:10.2118/171797-MS
11. Karimi, S., Saidian, M., Prasad, M., & Kazemi, H. (2015, September 28). Reservoir Rock Characterization Using Centrifuge and Nuclear Magnetic Resonance: A Laboratory Study of Middle Bakken Cores. Society of Petroleum Engineers. doi:10.2118/175069-MS
12. Li, H., Hart, B., Dawson, M., & Radjef, E. (2015, August 4). Characterizing the Middle Bakken: Laboratory Measurement and Rock Typing of the Middle Bakken Formation. Society of Petroleum Engineers. doi:10.2118/178676-MS
13. North Dakota Industrial Commission. Department of Mineral. Oil and Gas Division Website https://www.dmr.nd.gov/oilgas/ (Accessed 2015-2016)
14. Purcell, W. R.: "Capillary Pressures-Their Measurement Using Mercury and the Calculation of Permeability Therefrom", Trans. AIME (1949) 186,39.
15. Robinson, J.W., LeFever, J.A., Gaswirth, S.B. 2011. The Bakken–Three Forks Petroleum System In The Williston Basin.The Rocky Mountain Association of Geologists
16. Rodrigues, E. S., & Callard, J. G. (2012, January 1). Permeability and Completion Efficiency Determination From Production Data In the Haynesville, Eagle Ford and Avalon Shales. Society of Petroleum Engineers. doi:10.2118/161335-MS

17. Sapmanee, K., 2011. Effects of pore proximity on Behavior and Production Prediction of Gas/Condensate. Master Thesis, Mewbourne School of Petroleum and Geological Engineering, University of Oklahoma, 2011.
18. Thomas, F. B., Bennion, D. B., & Bennion, D. W. (1991, January 1). Recent Developments In Laboratory Data Sets For Determination Of Miscibility Limits. Petroleum Society of Canada. doi:10.2118/91-4
19. Thomeer, J. H. (1983, April 1). Air Permeability as a Function of Three Pore-Network Parameters. Society of Petroleum Engineers. doi:10.2118/10922-PA
20. Thomeer, J. H. M. (1960, March 1). Introduction of a Pore Geometrical Factor Defined by the Capillary Pressure Curve. Society of Petroleum Engineers. doi:10.2118/1324-G
21. Wattenbarger, R. A., El-Banbi, A. H., Villegas, M. E., & Maggard, J. B. (1998, January 1). Production Analysis of Linear Flow Into Fractured Tight Gas Wells. Society of Petroleum Engineers. doi:10.2118/39931-MS
22. Wells, J. D., & Amaefule, J. O. (1985, January 1). Capillary Pressure and Permeability Relationships in Tight Gas Sands. Society of Petroleum Engineers. doi:10.2118/13879-MS

Appendix A: Nomenclature

API	Stock Tank Oil Gravity
B_{oi}	Oi Formation Volume Factor at Initial Pressure, rb/stb
C_{fD}	Dimensionless Fracture Conductivity
c_t	Total Compressibility, 10^{-6} psi^{-1}
c_f	Rock /Formation Compressibility, 10^{-6} psi^{-1}
F_g	Thomeer's Pore Geometrical Factor
GOR	Gas Oil Ratio, scf/stb
GOR_{LF}	Linear Flow Gas Oil Ratio, scf/stb
G_p	Cumulative Gas Production, Mscf
G_{pelf}	Cumulative Gas Production at End of Linear Flow Time, Mscf
h	Reservoir Thickness, ft
k	Permeability, mD
k_a	Air Permeability, mD
k_e	Effective Permeability, mD
k_r	Relative Permeability
k_{rg}	Relative Permeability of Gas
k_{rnw}	Non-wetting Phase Relative Permeability
k_{ro}	Relative Permeability of Oil
k_{rw}	Wetting Phase Relative Permeability
LGR	Local Grid Refinement
m_{rcc}	Slope of 1/q versus Cumulative Production, D/stb
n_o	Oil Saturation Exponent
n_w	Wetting phase Saturation Exponent
N_p	Cumulative Oil Production, stb
N_{pelf}	Cumulative Oil Production at End of Linear Flow Time, stb
P_b	Bubble Point Pressure, psi
P_c	Capillary Pressure, psi
P_d	Mercury Displacement Pressure, psi
P_{fp}	Pressure at which fluid properties are measured, psi
P_i	Initial Reservoir Pressure, psi
PVT	Pressure Volume Temperature
P_{wf}	Flowing Bottom Hole Pressure (BHFP), psi
$1/q$	Reciprocal Oil Rate, $stbd^{-1}$
$1/q_i$	Reciprocal Rate Intercept on 1/q versus Cumulative Production, $stbd^{-1}$
R_{si}	Initial gas solubility, scf/stb
S_b	Mercury Saturation at Pressure P_c, percent bulk volume
$S_{b\infty}$	Mercury Saturation at Infinite Pressure percent bulk volume
S_g	Gas Saturation, fractional
S_{nw}	Non wetting Phase Saturation, percent pore volume
S_o	Oil Saturation, fractional
S_{oe}	Normalized oil saturation, fractional

S_{or} Residual Oil Saturation, fractional
S_w Wetting Phase Residual Saturation, percent pore volume
T Temperature, °F
t_{elf} Time to End of Linear Flow, Days
x_f Fracture Half-length, ft
y_e Distance from Fracture to Outer (No-Flow) Boundary, ft
y_{eD} Dimensionless Distance
ΔP $P_i - P_{wf}$

Greek Symbols

γ_{ws} Well Stream Gravity

γ_g Specific Gravity of Primary Separator Gas (Air=1).

γ_o Specific Gravity of Oil (Water=1).
ϕ Porosity, fractional
σ Interfacial tension, dynes/cm
μ Liquid Viscosity, cP
λ Slope of Log-Log Plot of S_{w^*} versus the Capillary Pressure P_c

Subscripts

c Critical
CP Constant Pressure
elf End of Linear Flow
f Fracture
g Gas
i Intercept and Initial
o Oil
Pfp Fluid Property Pressure
w Wetting